Lithos 127 (2011) 239–260

Contents lists available at SciVerse ScienceDirect

Lithos

journal homepage: www.elsevier.com/locate/lithos

Kwangsian crustal anatexis within the eastern South China Block: Geochemical, zircon U–Pb geochronological and Hf isotopic fingerprints from the gneissoid granites of Wugong and Wuyi–Yunkai Domains

Yuejun Wang [a,c,*], Aimei Zhang [a], Weiming Fan [a], Guochun Zhao [b], Guowei Zhang [c], Yuzhi Zhang [a], Feifei Zhang [a], Sanzhong Li [d]

[a] State Key Laboratory of Isotope Geochemistry, Guangzhou Institute of Geochemistry, Chinese Academy of Sciences, Guangzhou 510640, China
[b] Department of Earth Science, the University of Hong Kong, Hong Kong
[c] State Key of Continental Dynamics, Department of Geology, the Northwest University, Xi'an, China
[d] College of Marine Geosciences, Ocean University of China, Qingdao, 266100, China

ARTICLE INFO

Article history:
Received 23 January 2011
Accepted 31 July 2011
Available online 12 August 2011

Keywords:
Zircon U–Pb geochronology
Hf isotopic composition
Whole rocks geochemistry
Kwangsian gneissoid granites
Intracontinental crustal anatexis
Eastern South China Block

ABSTRACT

Gneissoid granites were traditionally thought to be the components of the Precambrian basement in the eastern South China Block, but twenty-four gneissoid granite samples from the Wugong, northern Wuyi, southern Wuyi and Yunkai Domains gave zircon U–Pb ages of 424–456 Ma, 410–457 Ma, 426–438 Ma and 415–450 Ma, respectively. The existence of the abundant Kwangsian gneissoid granites, which have incorrectly been assigned to the Precambrian basement, indicates that the "so-called" Precambrian stratigraphic sequence of the Cathaysia Block should be termed "Complex" rather than "Group". These gneissoid granites are peraluminous granites with relatively high Al_2O_3, MgO, TiO_2, FeOt and CaO/Na_2O but low CaO, $Al_2O_3/(MgO + FeOt)$ and Rb/Sr ratios. They exhibit strongly negative Ba, Sr, Nb, P and Ti and positive Pb anomalies in primitive mantle-normalized diagrams, and have initial $^{87}Sr/^{86}Sr$ ratios ranging from 0.70924 to 0.72935 and negative εNd(t) values from −6.4 to −11.4, similar to those of paragneissic enclaves and Precambrian sedimentary rocks in the eastern South China Block. The zircons crystallized in the Kwangsian gneissoid granites gave εHf(t) values ranging from +2.4 to −19.4 with the peak at −4 (almost all grains clustering at −1 to −12) and Hf model ages of 1.1–2.1 Ga. The synthesis of these geochemical and in-situ zircon Hf isotopic data indicates that the Kwangsian gneissoid granites dominantly originated from Proterozoic metapelitic and meta-igneous components with insignificant input of juvenile mantle-derived magmas. A model of two-stage crustal anatexis is proposed for the Kwangsian granitic magma in the eastern South China Block, with (1) the formation of 460–430 Ma granite through the breakdown of hydrous minerals under the condition of the doubly thickened crust, and (2) the generation of the 430–400 Ma granite accompanying promoted melting along a path of isothermal decompression due to the increasing thermal weakening for the collapse of the thickened crust. The crustal anatexis has probably occurred in an intracontinental tectonic regime that was geodynamically linked to the far-field response to the assembly of the Australian–Indian plate with the Cathaysia Block during middle Paleozoic (Kwangsian) time.

1. Introduction

The South China Block (SCB) consists of the Yangtze (also named Yangtze Platform) and Cathaysia (previously also termed Cathaysia Fold Belt) Blocks (Fig. 1), which amalgamated during Neoproterozoic time (e.g., Li et al., 1995, 2002, 2008; Zhao and Cawood, 1999). The SCB was subsequently overprinted by at least three tectonothermal events in the middle Paleozoic (~420–460 Ma), Triassic (Indosinian) and Jurassic–Cretaceous (Yanshanian) (e.g., Chen, 1999; Haynes, 1988; Li, 1998; Ren, 1991; Wang et al., 2003, 2008). The tectonic regime of the Indosinian and Yanshanian events in the SCB has extensively been discussed since the 1980s, especially in the last 20 years (e.g., Shu et al., 2008a, 2008b; Wang et al., 2007a, 2007b and references therein). However, the middle Paleozoic (late Ordovician–Silurian) tectonic process has not been well constrained (e.g., Charvet et al., 1996, 1999, 2010; Haynes, 1988; Shu et al., 1991; Wang et al., 2010). This tectonic event is traditionally referred to as the Caledonian Orogeny in the Chinese literature in comparison with the Caledonian Orogen of Europe (e.g., Huang, 1978; Huang et al., 1987; Ren, 1991). Li et al. (2010c) interpreted it as the Wuyi–Yunkai orogeny (also see

* Corresponding author at: Guangzhou Institute of Geochemistry, Chinese Academy of Sciences, P.O. Box 1131, Guangzhou 510640, People's Republic of China. Tel.: +86 20 85290527; fax: +86 20 85290708.
E-mail address: yjwang@gig.ac.cn (Y. Wang).

0024-4937/$ – see front matter © 2011 Elsevier B.V. All rights reserved.
doi:10.1016/j.lithos.2011.07.027

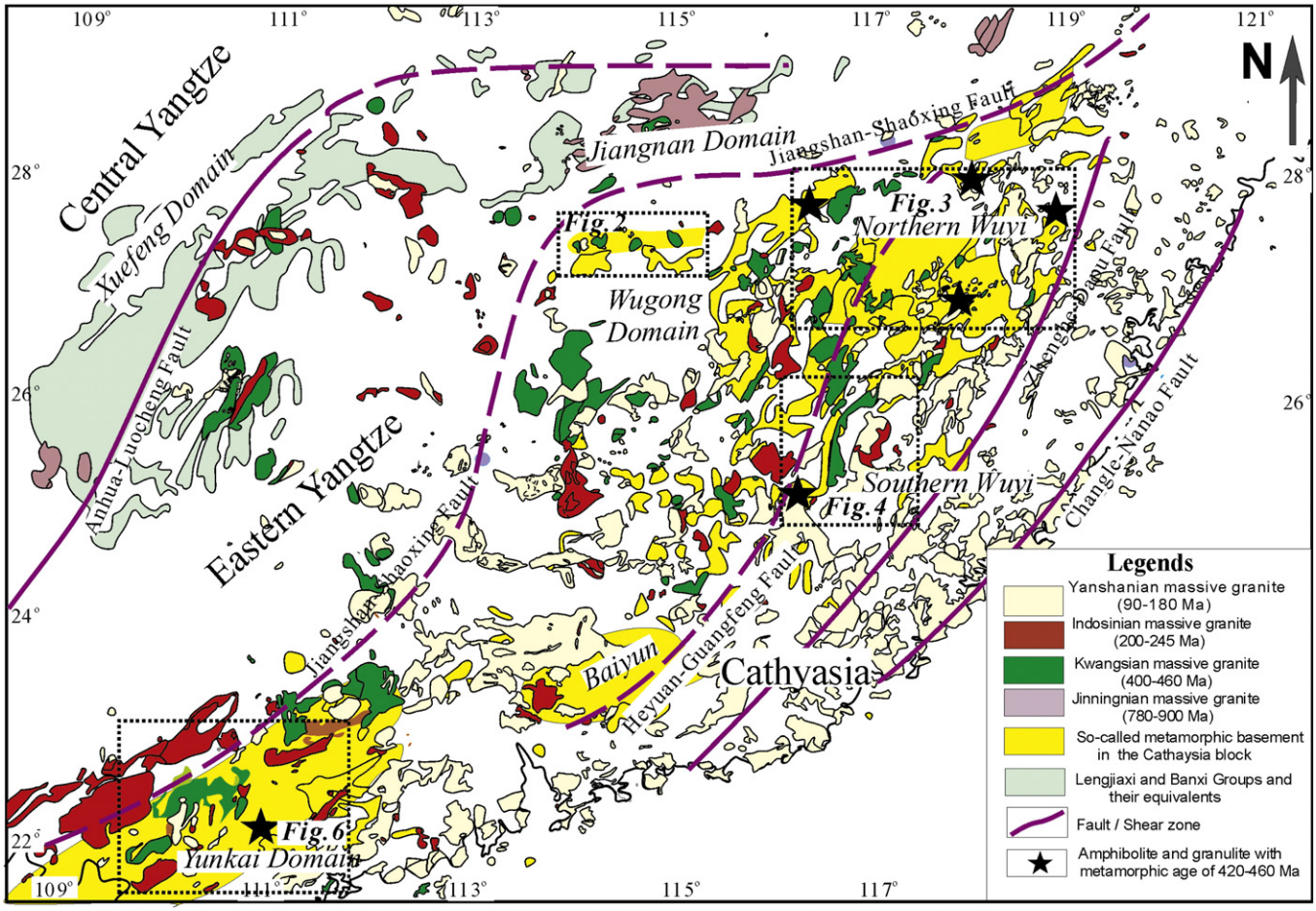

Fig. 1. A simplified geological map showing the distribution of the massive granitic plutons in the eastern South China Block and the "so-called" Precambrian basement (represented by gneissoid rocks, migmatite and amphibolites) in the Cathaysia Block (revised from Wang et al., 2007a, 2007b; Shu et al., 2008a, 2008b; Zhou et al., 2006, 2007). Also shown are the Wugong, northern Wuyi, southern Wuyi and Yunkai Domains.

Yang et al., 2010). In fact, this event was firstly termed as "the Kwangsian movement or Kwangsian orogeny" by Ting (1929). It is marked by an angular unconformity between the pre-Silurian and post-Lower Devonian sequences. Chen et al. (2010) and Wang et al. (2010) re-used the "Kwangsian orogeny" to define the middle Paleozoic event in the eastern SCB, which is herein adopted. It remains unknown or controversial as to the nature of the middle Paleozoic tectonic regime, with some authors suggesting an

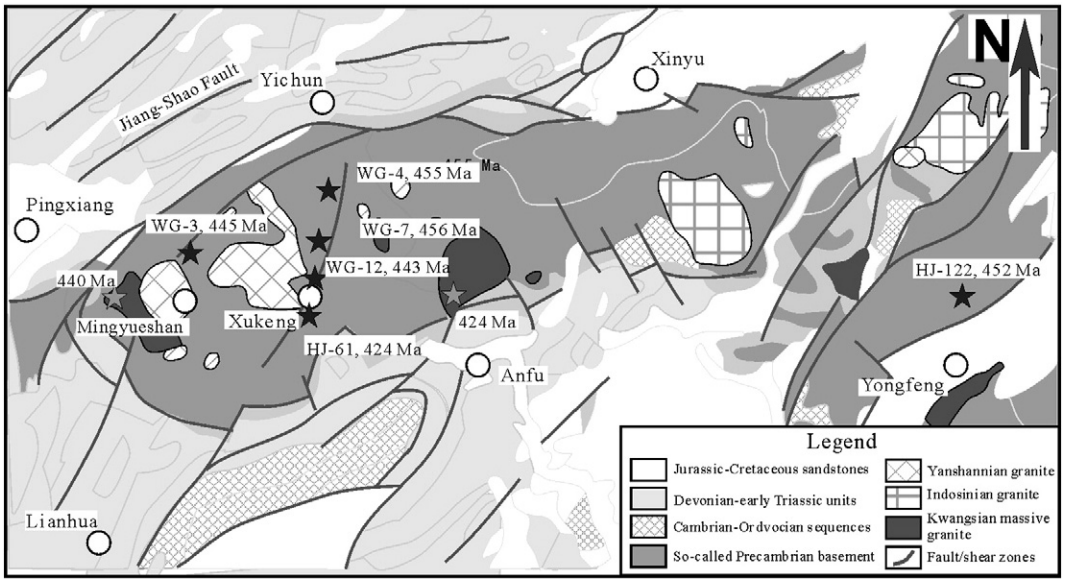

Fig. 2. Geological map of the Wugong Domain showing the gneissoid rocks, revised from the 1:1,000,000 geological map of Jiangxi Province (revised from Jiangxi BGMR, 1984). The quinquangular symbols refer to sampling locations for zircon U–Pb analyses in Fig. 3.

Table 1
Summary of lithology, sampling locations and zircon U–Pb geochronology of the dated samples from the eastern South China Block.

Sample	Lithology	Sampling location	Inherited zircon age	Crystallization age	$\varepsilon_{Hf}(t)$	T_{DM} model age
Wugong Domain						
09WG-3	Gneissoid granite	Mingyueshan, Yichun E114°16.775′,N27°42.099′		445 ± 8 Ma, n = 25, MSWD = 1.3	−3.5 to −10.7	1.39 to 1.74 Ga
09WG-4	Gneissoid granite	Nanmiao, Yichun E114°25.275′,N27°41.661′	510–526 Ma (n = 3), 911 ± 40 Ma, 841 ± 45 Ma	455 ± 9 Ma, n = 15, MSWD = 1.4	−1.4 to −16.6	1.29 to 2.04 Ga
09WG-7	Orthogneiss	North Zhangzhuan, Anfu E114°22.936′,N27°34.442′	938 ± 29 Ma (n = 3), 2261–2649 Ma (n = 3)	456 ± 5 Ma, n = 23, MSWD = 2.2	−14.4 to +1.3	1.14 to 1.94 Ga
09WG-12	Orthogneiss	Zhangzhuang, Anfu E114°22.993′,N27°33.203′		443 ± 5 Ma, n = 23, MSWD = 1.6	−0.0 to −18.9	1.21 to 2.14 Ga
07HJ-61	Gneissoid granite	Fukeng, Anfu, E114°20.290′,N27°31.877′	Inherited age: 747 Ma and 763 Ma, metamorphic age: 428 ± 3 Ma, n = 10, MSWD = 0.6	424 ± 6 Ma (n = 9, MSWD = 1.7)	−6.5 to −14.6	1.52 to 1.92 Ga
07HJ-122	Migmatite	Tancheng, Yongfeng E115°31.487′,N27°28.153′	534 Ma, 546 Ma, 842 Ma (n = 3)	452 ± 4 Ma, n = 9, MSWD = 3.1	−0.6 to −4.6	1.27 to 1.45 Ga
Northern Wuyi Domain						
09WG-25	Gneissoid granite	Huangpo, Yihuang E116°06.800′,N27°19.576′	639 Ma, 849 Ma, 818 Ma and 644 Ma	410 ± 10 Ma, n = 21, MSWD = 2.4	−2.3 to −9.1	1.27 to 1.67 Ga
08WY-6	Orthogneiss	Cizhou, Yeyang E117°26.873′,N28°10.496′		427 ± 15 Ma, n = 13, MSWD = 3.0		
09WG-57	Gneissoid granite	Qinyuan, Lishui E118°55.573′,N27°44.588′		430 ± 9 Ma, n = 14, MSWD = 2.3		
09WG-32 g	Leucosome in migmatite	City gardon, Lichuang E116°54.369′,N27°17.104′	803 ± 16 Ma, 1584 Ma, 2004 Ma and 1726 Ma	457 ± 6 Ma, n = 13, MSWD = 0.8	−1.3 to −15.6	1.29 to 2.00 Ga
09WG-32f	Migmatite	City gardon, Lichuang E116°54.369′,N27°17.104′	Inherited age: 799 Ma (n = 10) and 925 Ma (n = 12) Metamorphic age: 454 ± 11 Ma, n = 7, MSWD = 2.1		−1.6 to −10.3	1.28 to 1.73 Ga.
09WG-32b	Paragneissic enclave	City gardon, Lichuang E116°54.369′,N27°17.104′	Age-peak n = 42; 790 Ma n = 45; ~927 Ma, 1112 Ma,1713 Ma and 2574 Ma			
Southern Wuyi Domain						
09WG-93	Gneissoid granite	Xiangli, Wuping E116°11.690′,N25°23.930′	1069 Ma, 846 Ma, 741 Ma and 703 Ma	430 ± 6 Ma, n = 20, MSWD = 2.8	−0.7 to −18.6	1.24 to 2.13 Ga
09WG-94	Gneissoid granite	Taoxi, Wuping E116°10.364′,N25°21.064′	619 Ma, 621 Ma and 2260 ± 16 Ma	438 ± 3 Ma, n = 19, MSWD = 1.2	0.0 to −14.0	1.21 to 1.91 Ga
09WG-96	Gneissoid granite	Maocung, Yongping E116°07.202′,N25°15.454′	832 ± 29 Ma (n− = 4), 963 Ma, 975 Ma, 2097 Ma	432 ± 6 Ma, n = 18, MSWD = 1.2	−1.6 to −8.2	1.29 to 1.62 Ga
08FJ-88A	Gneissoid granite	Zhudongyang, Yong'an	746 ± 13 Ma	427 ± 4 Ma, n = 18, MSWD = 1.80	−2.9 to −18.7	1.34 to 2.12 Ga
08FJ-131B	Orthogneiss	Beijia village, Shanghang	560–624 Ma, 1551 ± 43 Ma and 2330 ± 61 Ma	426 ± 6 Ma, n = 16, MSWD = 0.3	−0.5 to −5.0	1.21 to 1.47 Ga
08FJ-135A	Gneissoid granite	North Yongping, Wuping	530 Ma, 547 Ma, 821 Ma and 1409 Ma	426 ± 8 Ma, n = 9, MSWD = 0.73	+0.6 to −8.5	1.17 to 1.63 Ga
08FJ-135B	Gneissoid granite	Yongping, Wuping	560–645 Ma, 1123 ± 16 Ma and 2550 ± 35 Ma	437 ± 3 Ma, n = 15, MSWD = 1.0		
08FJ-136	Orthogneiss	North Yongping, Wuping	2584 Ma, 1731 Ma, 757 Ma and 738 Ma	430 ± 6 Ma, n = 14, MSWD = 1.3	−0.4 to −8.6	1.22 to 1.62 Ga
Yunkai Domain						
09YK-8B	Orthogneiss	Yunlong, Xingyi E111°01.095′,N22°30.157′	Metamorphic age: 203 ± 10 Ma (Th/U = 0.02)	450 ± 8 Ma, n = 13, MSWD = 1.7	+1.3 to −5.0	1.15 to 1.46 Ga
09YK-10a	Gneissoid granite	Jintong, Xinyi E110°46.000′,N22°25.347′		449 ± 5 Ma, n = 26, MSWD = 1.6	+2.4 to −5.1	1.12 to 1.47 Ga
09YK-12	Orthogneiss	Licun, Rongxian E110°41.596′,N22°36.153′	Metamorphic age: 23 9 ± 6 Ma (Th/U = 0.18)	443 ± 7 Ma, n = 22, MSWD = 2.6	−0.6 to −8.7	1.22 to 1.62 Ga
09YK-15a	Gneissoid granite	Shiwo, Beiliu E110°25.386′,N22°12.851′	811–943 Ma (n = 4)	415 ± 7 Ma, n = 22, MSWD = 3.9	+0.2 to −12.4	1.17 to 1.82 Ga
09YK-16 T	Leucosome in migmatite	Xieji, Gaozhou E111°01.002′,N21°54.561′		435 ± 8 Ma, n = 27, MSWD = 1.8	−3.8 to −16.9	1.38 to 2.02 Ga
09YK-16 K	Paragneiss	Xieji, Gaozhou E111°01.002′,N21°54.561′	Age-peak: n = 58; 514 Ma, 823 Ma, 947 Ma, 1150 Ma, 1776 Ma			
09YK-17	Orthogneiss	Xintong, Gaozhou E111°08.155′,N21°52.369′	787 ± 14 Ma (n = 3), 518 ± 14 Ma (n = 3), 1282 Ma	452 ± 6 Ma, n = 16, MSWD = 1.5	−7.2 to −14.7	1.58–1.96 Ga

intracontinental model (e.g., Charvet et al., 1999, 2010; Chen et al., 2000; Li et al., 2010a, 2010b, 2010c; Shu et al., 1991; Shu et al., 2008a, 2008b; Wang et al., 2007a, 2007b, 2010), whereas others have considered a subduction regime related to the closure of an inferred early Paleozoic Huanan ocean (e.g., Chen et al., 2006; Hsű et al., 1990; Liu and Xu, 1994; Ma et al., 2004). This debate results from poor constraints on the geological signatures associated with the Kwangsian orogenesis in the SCB.

The extensive occurrence of granitic rocks is one of the remarkable geological signatures associated with the Kwangsian orogenic event in the eastern SCB (e.g., Hunan Bureau of Geology and Mineral Resources (BGMR), 1988; Jiangxi BGMR, 1985; Fujian BGMR, 1985; Guangdong BGMR, 1988; Haynes, 1988; Shu et al., 1991, 2008a, 2008b; Charvet et al., 1996, 1999, 2010; Wang et al., 2007a, 2007b). The origin of these granitic rocks is considered as a key to better understand the early–middle Paleozoic tectonic evolution of the SCB. However, little attention has been paid to the geochronology, petrogenesis and tectonic implications of these Kwangsian granitic rocks. Available data show that the Kwangsian granitic rocks in the SCB can be subdivided into gneissoid and massive granites defined as the granites with and without a strong magmatic orientation, respectively. The massive granites are commonly regarded as being of large volume and mainly occur as laccoliths and batholiths (e.g., Chen and Jahn, 1998; Huang, 1978; Huang et al., 1987; Hunan BGMR, 1988; Jiangxi BGMR, 1984). They are mainly S-type peraluminous granites that originated from crustal materials (e.g., Charvet et al.,

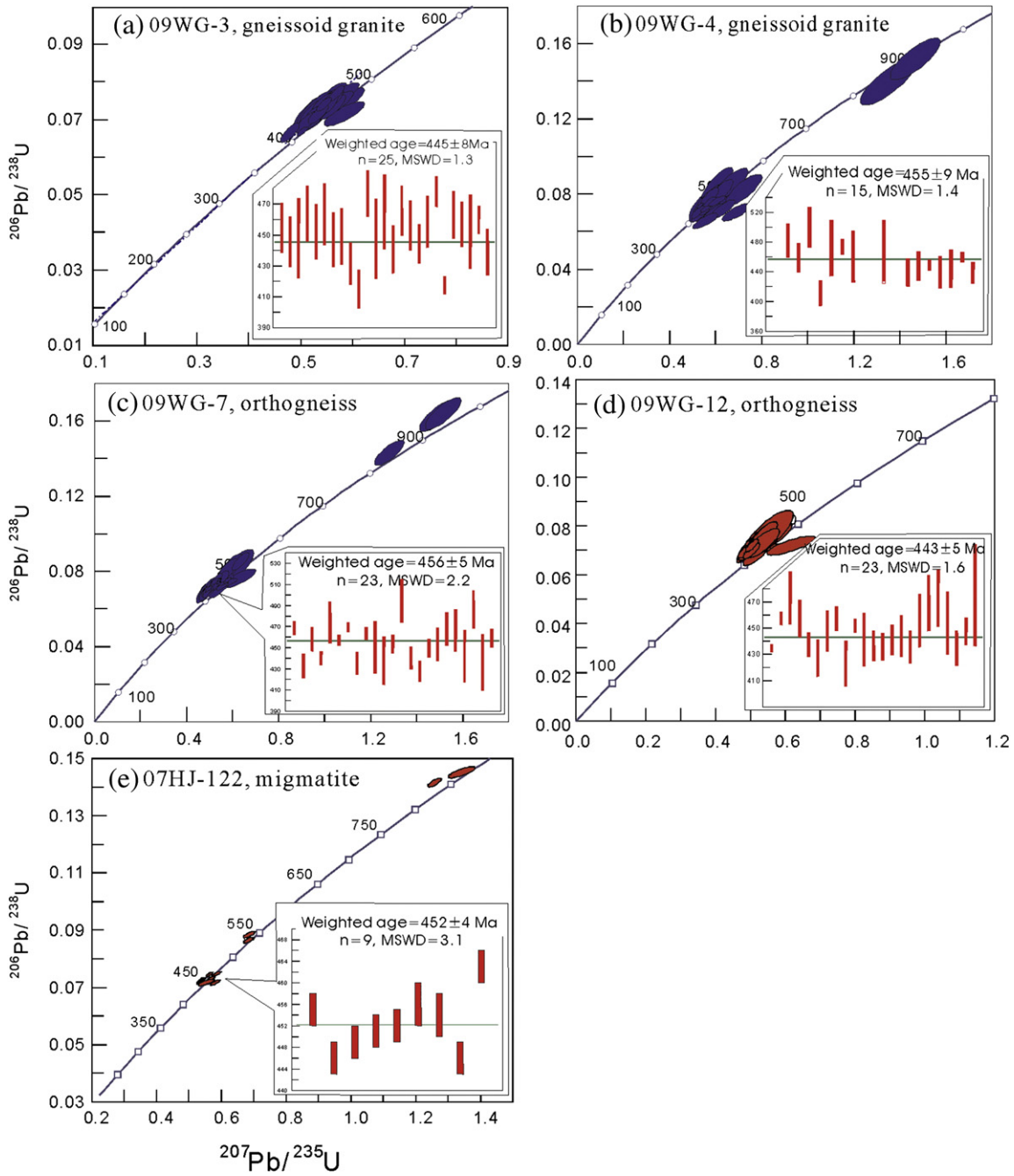

Fig. 3. (a–g) Concordia diagrams of zircon U–Pb data for the representative samples from the Wugong Domain. (a) 09WG-3 gneissoid granite (Mingyueshan, Yichun); (b) 09WG-4 gneissoid granite (Nanmiao, Yichun); (c) 09WG-7 orthogneiss (North Zhangzhuan, Anfu); (d) 09WG-12 orthogneiss (Zhangzhuang, Anfu); (e) 07HJ-122 migmatite (Tancheng, Yongfeng). The locations for these samples are shown in Fig. 2.

1999, 2010; Chen and Jahn, 1998; Li et al., 2010c; Zhang et al., 2010a, 2010b and reference therein). The associated gneissoid granites were traditionally considered to be of less volume and predominantly outcrop in several areas of the Wugong and northern Wuyi Domains, (e.g., Jiangxi BGMR, 1984). Recently geochronological data show that some orthogneiss (defined by the granite with post-magmatic ductile deformation) and gneissoid granites, which are jointly called as gneissoid granite in the Chinese literature (also is herein adopted), as well as the leucosome in migmatite from the Yunkai, Wuyi and Baiyun Domains are not the Precambrian basement as traditionally thought but the products of the crustal anatexis during the Ordovician and early Devonian period (e.g., Charvet et al., 1996, 1999, 2010; Li et al., 2010c; Wan et al., 2007, 2010; Wang et al., 2007b; Yang et al., 2010). It is very likely that the abundant Kwangsian gneissoid granites exist but are incorrectly assigned to the "so-called" Precambrian basement of the eastern SCB. Therefore, more precise geochronological data are needed. Additionally, little is known about the temporal and spatial patterns of the Kwangsian gneissoid granites and their tectonic implications. In this study, we present U–Pb geochronological and Hf isotopic data and their elemental and Sr–Nd isotopic results of twenty-seven gneissoid granite samples from the Wugong, northern and southern Wuyi and Yunkai metamorphic Domains in the eastern SCB. These data place constraints on the petrogenesis of the Kwangsian gneissoid granites and provide important insights into understanding crustal anatexis in the intracontinental regime of the eastern SCB.

2. Geological setting and petrography

The Kwangsian, Indosinian and Yanshanian massive granites predominantly crop out in a large area to east of the Anhua–Luocheng Fault as shown in Fig. 1 (e.g., Fujian BGMR, 1985; Jiangxi BGMR, 1984; Wan et al., 2007, 2010; Yu et al., 2007b) where is usually referred as the eastern SCB. In the Yangtze Block, the granites are only exposed in the areas between the Jiangshan–Shaoxing and Anhua–Luocheng Faults, where is also called as the eastern Yangtze Block. In the Cathaysia Block, they extensively crop out in the areas to east of the Jiangshan–Shaoxing Fault. The crystalline basement of the eastern Yangtze Block has an affinity to the central Yangtze Block that consists of Neoarchaean and Paleoproterozoic TTG rocks, felsic gneisses and amphibolites (e.g., Gao et al., 1999; Qiu et al., 2000). The Cathaysia basement is conventionally considered to be of Paleo- to Mesoproterozoic origin and is composed mainly of greenschist- to amphibolite-facies schist, gneiss, migmatite and amphibolite (e.g., Badu, Longquan, Mayuan and Yunkai "Groups"; Liu et al., 2008; Yu et al., 2009, 2010).

Following the Jinningian (Neoproterozoic) amalgamation of the Yangtze and Cathaysia Blocks, a late Neoproterozoic failed rift with a >13 km thick abyssal marine deposition was developed (e.g., Hunan

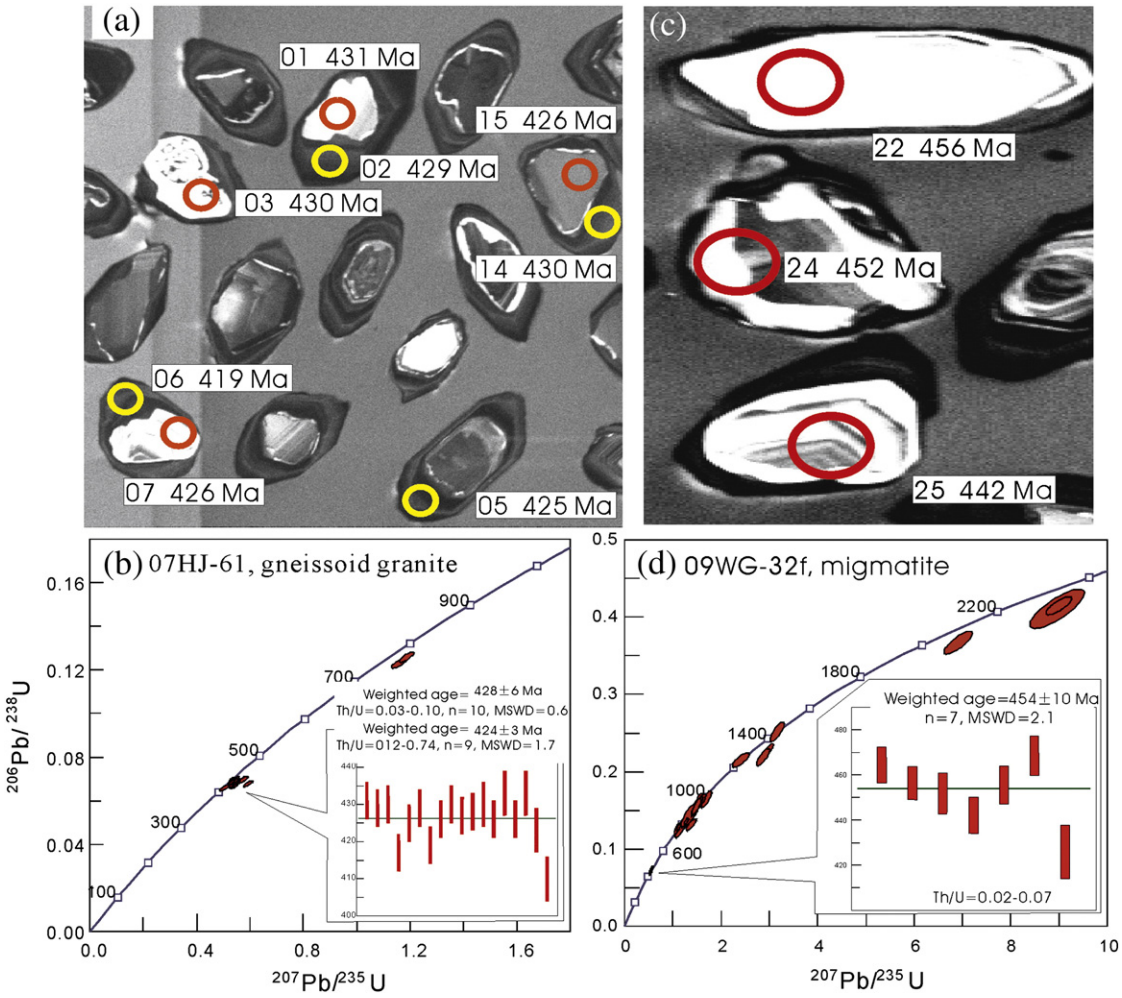

Fig. 4. (a–b) CL image of the representative zircons showing the metamorphic core and oscillatory rim from 07HJ-61 and 09WG-32f, respectively. (c–d) Concordia diagrams of zircon U–Pb data for the 07HJ-61 gneissoid granite (Fukeng, Anfu) from the Wugong Domian and 09WG-32f migmatite enclave into the Kwangsian granitic pluton (Lichuang) from the northern Wuyi Domain, respectively.

BGMR, 1988; Wang and Li, 2003). The rift is tectonically located at an area between the Xuefeng and Wuyi- Baiyun-Yunkai Domains (Fig. 1), geographically extending from Hunan, through Jiangxi and western Guangdong, to eastern Guangxi Provinces (e.g., Hunan BGMR, 1988; Jiangxi BGMR, 1984; Wang and Li, 2003). The lower Paleozoic packages in the region are characterized by an interstratified carbonate–siliciclastic succession in the eastern Yangtze and a siliciclastic succession in the Cathaysia Blocks, which are overlain by an upper Paleozoic succession across an angular unconformity.

The Kwangsian massive granitic plutons predominantly outcrop in the areas between the Anhua–Luocheng and Heyuan–Guangfeng faults (Fig. 1). These granites intrude the pre-Silurian strata as stocks and batholiths (e.g., Hunan BGMR, 1988; Jiangxi BGMR, 1984). They are mainly coarse- to medium-grained monzonite, two-mica granites, biotite granite and garnet-bearing granites with insignificant deformation. The biotite granodiorite and hornblende granite are rare. On the other hand, the gneissoid granites are traditionally considered to be of small volume. They show a strong magmatic orientation or a post-magmatic ductile deformational texture and are mainly characterized by muscovite-, or garnet- or tourmaline-bearing granites. The most common mineral assemblage is plagioclase (~30–40%), K-feldspar (~15–25%), quartz (~35–45%) and biotite (~5–10%) with minor amounts of muscovite and accessory minerals (e.g., garnet, tourmaline, apatite, zircon, and monazite and Fe–Ti oxides). The proportions of alkali feldspar to plagioclase are variable. There are abundant angular to rounded enclaves (mainly paragneiss and amphibolite) in the gneissoid granites. At Nandu in the Yunkai Domain, an gneissoid granite is directly overlain by the Devonian sandstone, as observed at Shanzhuang (Wugong) and Doushui (Wuyi) where the middle Devonian sandstone uncomfortably overlaid the Silurian massive granite. Recent geochronological data show that some gneissoid rocks might also be of Kwangsian origin in the Wugong and Wuyi–Baiyun–Yunkai metamorphic Domains (Wan et al., 2007, 2010; Wang et al., 2007b; Yang et al., 2010) in which they were mapped as the main exposures of the Proterozoic Badu, Chencai, Mayuan and Yunkai "Groups" (e.g., Fujian BGMR, 1985; Guangdong BGMR, 1988; Wan et al., 2007, 2010; Yu et al., 2009).

3. Analytical methods

Zircon grains for U–Pb dating and Hf isotopic compositions were separated using conventional heavy liquid and magnetic techniques. Zircons were then handpicked under a binocular microscope, mounted on adhesive tape, enclosed in epoxy resin and polished, and then photographed in reflected and transmitted light. The cathode-luminescence (CL) imaging was carried out using a JXA-8100 Electron Probe Microanalyzer with a Mono CL3 CL System for high resolution imaging and spectroscopy at the Guangzhou Institute of Geochemistry (GIG), Chinese Academy of Sciences (CAS).

The U–Pb isotopic determination for 27 samples was performed on the polished mount using a Laser ICP-MS at the Institute of Geology and Geophysics (IGG), CAS and Hong Kong University. Spot size in the range of 40–50 μm was used for data collection. The standard CN92-2, 91500 and GJ zircons were used to calibrate the U–Th–Pb ratios and absolute U abundances. The instrumental setting and detailed analytical procedure have been described by Xia et al. (2004). The errors for individual U–Pb analyses are presented with 1σ error in data tables and in concordia diagrams and uncertainties in age results are quoted at 95% level (2σ). Data processing was carried out using the SQUID 1.03 and Isoplot/Ex 2.49 programs of Ludwig (2001).

Zircon in-situ Hf isotopic analysis was carried out using a Geolas-193 laser-ablation microprobe, attached to a Neptune multi-collector ICP-MS at the IGG, CAS. External calibration was made by measuring zircon standard 91500 with the unknowns during the analyses to evaluate the reliability of the analytical data, which yielded a weighted mean $^{176}Hf/^{177}Hf$ ratio of 0.282307 ± 31 (2σ, Wu et al., 2006). This value is in good agreement with the recommended value of 0.282305 ± 12 (2σ, Nebel-Jacobsen et al., 2005). The mean β_{Yb} value was applied for the isobaric interference correction of ^{176}Yb on ^{176}Hf in the same spot. The ratio of $^{176}Yb/^{172}Yb$ (0.5887) was also applied for the Yb correction.

Major oxides were determined by X-ray fluorescence spectrometry at the GIG, CAS. Trace element analyses were performed at the GIG, CAS by an inductively coupled plasma mass spectrometry (ICPMS). About 100 mg samples are digested with 1 ml of HF and 0.5 ml HNO_3 in screw top PTFE-lines stainless steel bombs at 190 °C

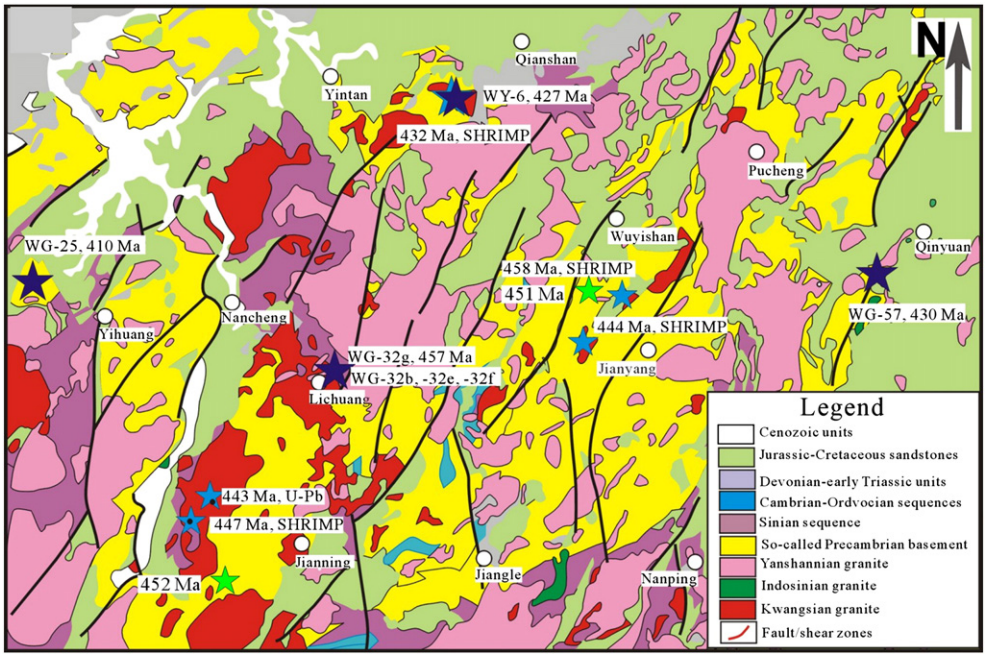

Fig. 5. Geological map in the Northern Wuyi Domain showing the so-called Precambrian basement rocks, revised from the 1:1,000,000 geological map of Jiangxi and Fujian Provinces (revised from Jiangxi BGMR, 1984; Fujian BGMR, 1985). The quinquangular symbol refers to sampling location for zircon U–Pb analyses in Fig. 6. The noted ages are from Li et al. (2010b, 2010c), Wan et al. (2007), Charvet et al. (2010) and Zeng and Liu (2000).

for 12 h. Analyses of Sr and Nd isotopic ratios were performed on the Micromass IsoProbe™ MC-ICPMS at the GIG, CAS. The total procedure blanks were in the range of 200–500 pg for Sr and <50 pg for Nd. The mass fractionation corrections for isotopic ratios are based on $^{86}Sr/^{88}Sr = 0.1194$ and $^{146}Nd/^{144}Nd = 0.7219$. The measured $^{87}Sr/^{86}Sr$ ratios of the SRM 987 standard and $^{143}Nd/^{144}Nd$ ratios of the La Jolla standard are 0.710265 ± 12 (2σ) and 0.511862 ± 10 (2σ), respectively.

4. Zircon U–Pb and Hf systematics

The representative gneissoid granites and associated paragneissic enclaves were collected from the Wugong, Northern and Southern Wuyi, and Yunkai Domains of the eastern SCB, respectively (Figs. 2, 5, 7 and 9). Twenty-seven of these samples were selected for the Laser probe ICP-MS or SIMS zircon U–Pb dating. The analytical results for zircon U–Pb and Hf isotopic compositions are listed in the Supplementary Datasets 1 and 2, respectively. Their sampling locations, lithology and dating results are summarized in Table 1 and Figs. 2–10. Zircons that were separated from the gneissoid granites exhibit mostly euhedral shapes with up to 150–350 μm in length with length/width ratios of 2:1–4:1. Most crystals are light brown or brown, prismatic and transparent to subtransparent, and exhibit internal structures with strong oscillatory zoning, typical of magmatic origin.

4.1. Wugong Domain

The samples from the Wugong Domain (Fig. 2) comprise three gneissoid granites (09WG-3 and -4 and 07HJ-61), two orthogneiss (09WG-7 and -12) and one migmatite (07HJ-122). They were previously

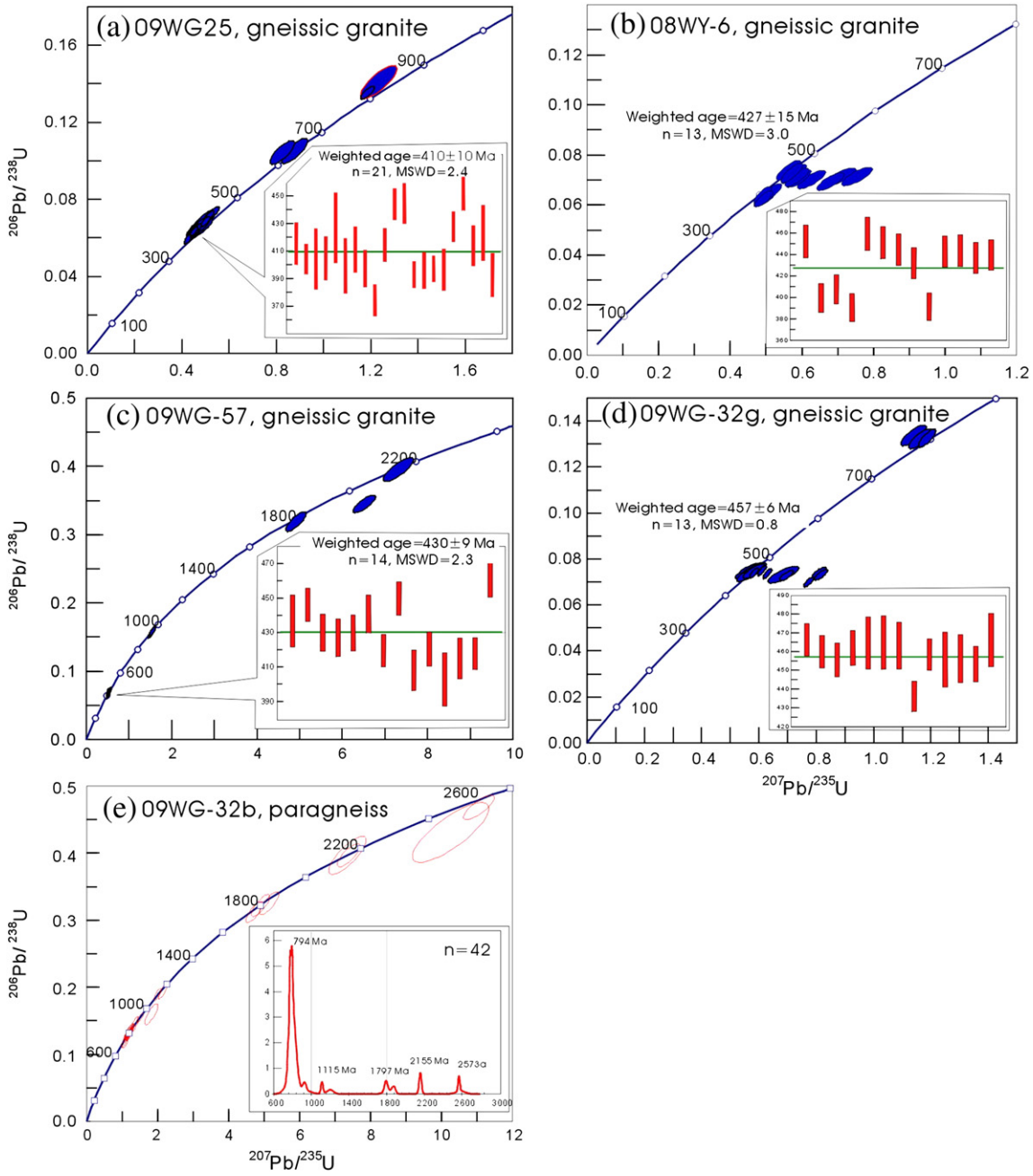

Fig. 6. (a–e) Concordia diagrams of zircon U–Pb data for the representative samples from the Northern Wuyi Domain. (a) 09WG-25 gneissoid granite (Huangpo, Yihuang); (b) 08WY-6 orthogneiss (Cizhou, Yeyang); (c) 09WG-57 gneissoid granite (Qinyuan, Lishui); (d) 09WG-32 g leucosome in migmatite (City gardon, Lichuang); (e) 09WG-32b paragneissic enclave into the Kwangsian granitic pluton (Lichuang). The locations for these samples are shown in Fig. 5.

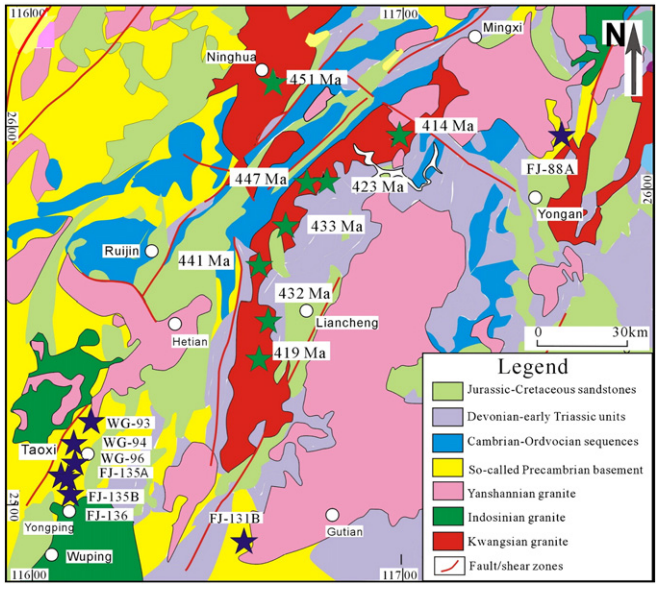

Fig. 7. Geological map showing the so-called Precambrian basement rocks in the southern Wuyi Domain, revised from the 1:1,000,000 geological map of Fujian Province (revised from Fujian BGMR, 1985). The quinquangular symbols refer to sampling locations for zircon U–Pb analyses. The noted ages are from Zhang et al. (2010a), Chen et al. (2008) and Charvet et al. (2010).

considered to be representative of Precambrian basement (e.g., Faure et al., 1996; Jiangxi BGMR, 1984).

Zircons with oscillatory zoning from 09WG-3, 09WG-04, 09WG-7 and 09WG-12 give weighted mean $^{206}Pb/^{238}U$ ages of 445 ± 8 Ma, 455 ± 9 Ma, 456 ± 5 Ma and 443 ± 5 Ma, respectively (Fig. 3a–d). Their εHf(t) values vary from −16.6 to +1.3 and T_{DM} model ages range from 1.1 to 2.1 Ga. Nine of 16 grains from 07HJ-122 yield a weighted mean age of 452 ± 4 Ma (Fig. 3e) with εHf(t) values of −0.6 to −4.6 and the T_{DM} model ages of 1.3–1.5 Ga.

Nineteen analyses from 07HJ-61 have εHf(t) values of −6.5 to −14.6 and T_{DM} model ages of 1.5–1.9 Ga. On CL images, ten of these grains show metamorphic rims surrounding poorly zoned cores (Fig. 4a). They have Th/U ratios of 0.03–0.10 and give a weighted mean $^{206}Pb/^{238}U$ age of 428 ± 3 Ma (Fig. 4c), interpreted as the metamorphic age. The remaining nine spots on the grains show strong oscillatory zonation and a concentric oscillatory rim and give a weighted mean age of 424 ± 6 Ma with Th/U ratios of 0.12–0.74 (Supplementary Dataset 1 and Fig. 4c), which represents the age of the crystallization zircons.

Older zircons also exist in these samples (Fig. 3b–e). Spots 09WG4-01, -11 and -12 and 07HJ-122-08 and -13 give $^{206}Pb/^{238}U$ apparent ages of 510–546 Ma, with εHf(t) values of −7.6 to −12.8 and T_{DM} of 1.64–1.91. The sample contains $^{206}Pb/^{238}U$ apparent ages of 747–979 Ma and 2159–2649 Ma, with the εHf(t) values of +0.72-+7.05 and -1.1-+2.1 and T_{DM} model ages of 1.1–1.6 Ga and 2.7–3.0 Ga, respectively, interpreted to be inherited from a magma source.

4.2. Northern Wuyi Domain

Samples 09WG-25 (Huangpo) and 09WG-57 (Qinyuan) are gneissoid granites collected from the northern Wuyi Domain (Fig. 5), traditionally mapped as the Proterozoic Mayuan "Group". Orthogneiss samples 08WY-6 and 09WG-32 g are from Cizhou and Lichuan (Fig. 5). Samples 09WG-32f and 09WG-32b are migmatite and paragneiss enclosed in the Lichuan granitic pluton, respectively.

One cluster defined by 21 analyses from 09WG-25 gives a weighted mean age of 410 ± 10 Ma (Fig. 6a) with Th/U ratios of 0.10–1.36. Their εHf(t) values vary from −9.1 to −2.3, and the T_{DM} model ages range from 1.3 to 1.7 Ga. The grains from 08WY-6, 09WG-57 and 09WG-32 g yield weighted mean $^{206}Pb/^{238}U$ ages of 427 ± 15 Ma, 430 ± 9 Ma, and 457 ± 6 Ma, respectively (Fig. 6b–d), interpreted as the crystallization age. The remaining grains give $^{206}Pb/^{238}U$ apparent ages of 639–644 Ma, 800–849 Ma, 932–948 Ma, 1726–1785 Ma, 1911–2147 Ma, respectively (Fig. 6a–d). These zircons are considered to be the inherited grains.

Seven of thirty-six grains from 09WG-32f (migmatitic enclave) show poorly zoning in CL images (Fig. 4b). They have Th/U ratios of 0.02–0.07 and yield a weighted mean age of 454 ± 11 Ma (Fig. 4d). These grains give εHf(t) values ranging from −10.3 to −1.6, and T_{DM} model ages from 1.3 to 1.7 Ga. Ten zircons form a cluster at 799 Ma with εHf(t) values of −6.1 ~ +6.9 and T_{DM} model ages of 1.1–1.8 Ga. Twelve grains yield an age peak at 925 Ma with almost all grains having positive εHf(t) values. The other six grains have $^{206}Pb/^{238}U$ apparent ages range between 1254 and 1444 Ma and 2013–2231 Ma, respectively. The 42 grains from 09WG-32b form a main age peak at ~790 Ma and three subordinate clusters at 1115 Ma, 1797 Ma and 2155 Ma, respectively (Fig. 5f). They have the Th/U ratios of higher than 0.20, variable εHf(t) values and Proterozoic T_{DM} model ages.

4.3. Southern Wuyi Domain

Eight gneissoid granites or orthogneiss were collected from the southern Wuyi Domain (Fig. 7) previously mapped as the Proterozoic or Sinian metamorphic rocks (e.g., Fujian BGMR, 1985). Zircons from 09WG-93, 09WG-94, 09WG-96, 08FJ-88A, 08FJ-131B, 08FJ-135A and 08FJ-136 give weighted mean $^{206}Pb/^{238}U$ ages of 430 ± 6 Ma, 438 ± 3 Ma, 432 ± 6 Ma, 427 ± 4 Ma, 426 ± 6 Ma, 426 ± 8 Ma and 430 ± 6 Ma, respectively (Fig. 8a–g and Table 1). Their εHf(t) values for these grains range from +0.6 to −18.7 and T_{DM} model ages from 1.2 to 2.1 Ga. The U–Pb isotopic data for zircons from the 08FJ-135B that was performed by a SIMS instrument at the Institute of Geology and Geophysics (CAS) form a major population and yield a weighted mean age of 437 ± 3 Ma (n = 15, MSWD = 1.0, Fig. 8h). The remaining grains from these samples are clustered into the age ranges of 530–645 Ma, 703–975 Ma, 1069–1123 Ma, 1409–1551 Ma, 1731 Ma and 2097–2330 Ma, respectively, interpreted to the ages of the inherited grains. These grains usually have positive εHf(t) values and Proterozoic (1.03–2.69 Ga) T_{DM} model ages.

4.4. Yunkai Domain

Five orthogneiss and gneissoid granites were sampled from the Yunkai Domain (Fig. 9), which were previously described as the Precambrian Yunkai "Group" (e.g., Guangdong BGMR, 1988; Guangxi BGMR, 1985; Qin et al., 2006). The zircons from these samples yield weighted mean ages of 450 ± 8 Ma (09YK–8B), 449 ± 5 Ma (09YK–10A), 443 ± 7 Ma (09YK–12A), 415 ± 7 Ma (09YK–15A) and 452 ± 6 Ma (09YK–17), respectively (Fig. 10 and Table 1). Their εHf(t) values range from −16.93 to +2.38 and T_{DM} model ages from 1.1 Ga to 2.0 Ga. It is noted that spots of 09YK-8B-13 and 09YK-12-15 yield the $^{206}Pb/^{238}U$ apparent ages of 203 ± 10 Ma (Th/U = 0.02, εHf(t) = +1.3) and 239 ± 6 Ma (Th/U = 0.18, $\varepsilon_{Hf}(t) = -2.9$), respectively. The two Indosinian ages can be interpreted as the metamorphic age (Fig. 10a and c). The Neoproterozoic ages between 674 Ma and 943 Ma and Mesoproterozoic age of 1282 Ma are also produced from the inherited zircons in these

Fig. 8. (a–h) Concordia diagrams of zircon U–Pb data for the representative samples from the southern Wuyi Domain. (a) 09WG-93 gneissoid granite (Xiangli, Wuping); (b) 08FJ-88A gneissoid granite (Zhudongyang, Yong'an); (c) 09WG-96 gneissoid granite (Maocung, Yongping); (d) 09WG-94 gneissoid granite (Taoxi, Wuping); (e) 08FJ-131B orthogneiss (Beijia, Shanghang); (f) 08FJ-135A gneissoid granite (Yongping, Wuping); (g) 08FJ-136 orthogneiss (North Yongping, Wuping); (h) 08FJ-135B gneissoid granite (Yongping, Wuping). The locations for these samples are shown in Fig. 7.

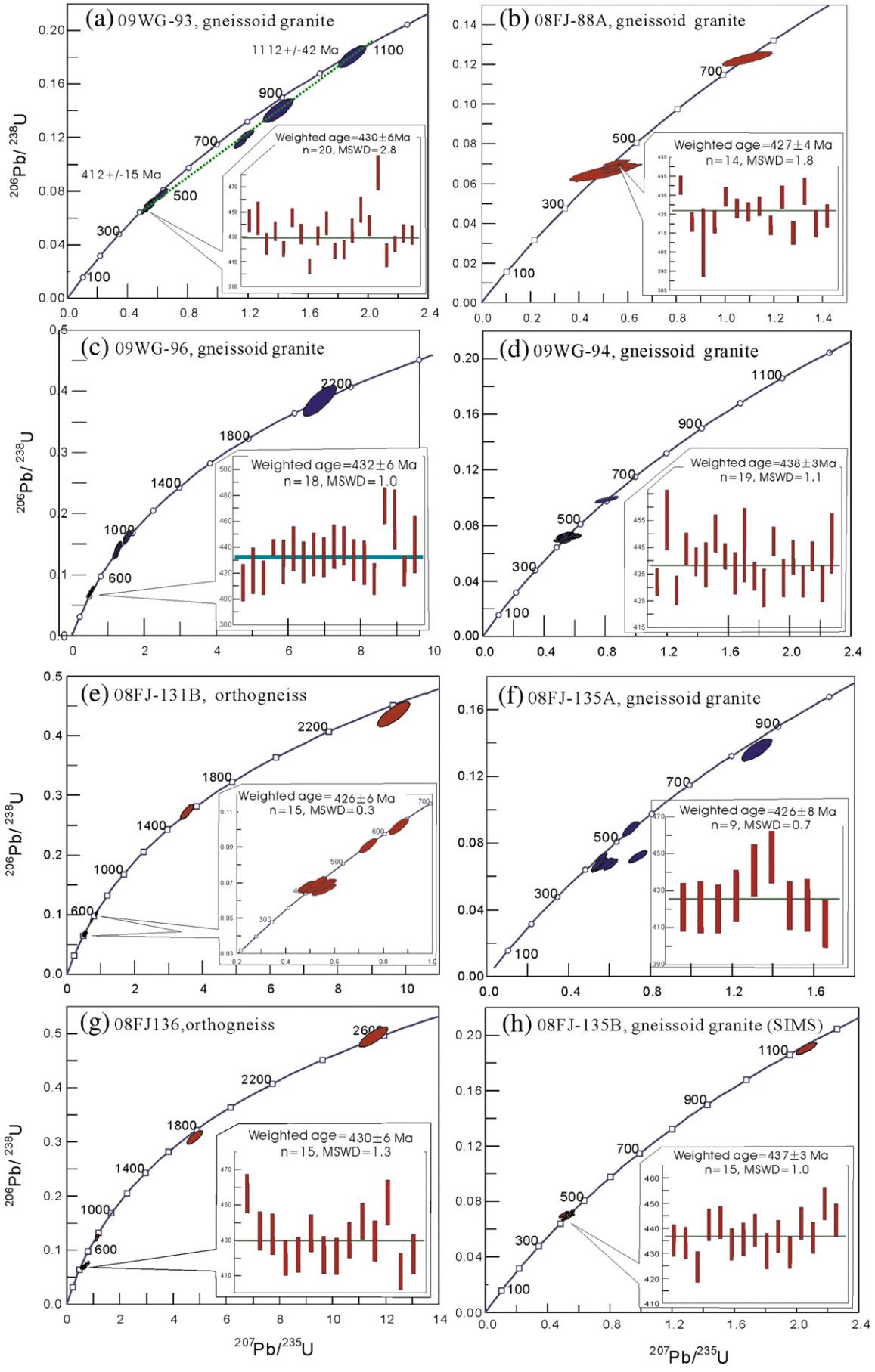
(a) 09WG-93, gneissoid granite
1112+/-42 Ma
412+/-15 Ma
Weighted age=430±6Ma
n=20, MSWD=2.8
(b) 08FJ-88A, gneissoid granite
Weighted age=427±4 Ma
n=14, MSWD=1.8
(c) 09WG-96, gneissoid granite
Weighted age=432±6 Ma
n=18, MSWD=1.0
(d) 09WG-94, gneissoid granite
Weighted age=438±3Ma
n=19, MSWD=1.1
(e) 08FJ-131B, orthogneiss
Weighted age=426±6 Ma
n=15, MSWD=0.3
(f) 08FJ-135A, gneissoid granite
Weighted age=426±8 Ma
n=9, MSWD=0.7
(g) 08FJ136,orthogneiss
Weighted age=430±6 Ma
n=15, MSWD=1.3
(h) 08FJ-135B, gneissoid granite (SIMS)
Weighted age=437±3 Ma
n=15, MSWD=1.0
206Pb/238U
207Pb/235U

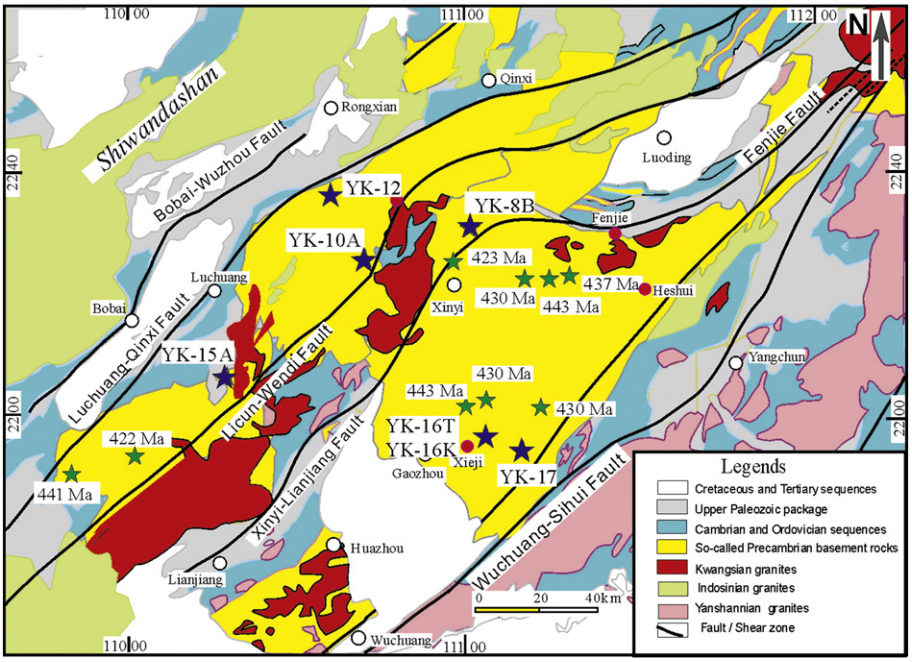

Fig. 9. Geological map showing the so-called Precambrian basement rocks in the Yunkai Domain, revised from the 1:1,000,000 geological map of Guangdong Province (revised from Guangdong BGMR, 1988). The quinquangular symbol refers to sampling location for zircon U–Pb analyses. The noted ages are from Wang et al. (2007b) and Wan et al. (2010).

samples. The leucosome (09YK–16 T) in migmatite from Xiejie (Gaozhou) gives a weighted mean age of 435 ± 8 Ma (Fig. 10e). Fifty eight analyses from 09YK–16 K (a paragneissic enclave at Xiejie) plot on or near the concordia curve (Fig. 10h) and give the five age-peaks of 630 Ma, 755 Ma, 947 Ma, 1190 Ma and 1766 Ma, with $\varepsilon_{Hf}(t)$ values ranging from −15.2 to +13.9 and T_{DM} model ages from 1.0 to 3.1 Ga.

5. Whole-rock geochemical results

The representative gneissoid granites from the Wugong, northern and southern Wuyi and Yunkai Domains were selected for elemental and Sr–Nd isotopic analyses. Their analytical results are presented in Table 2.

Almost all of our samples are strongly peraluminous. Together with the data presented by Wan et al. (2010) and Zeng et al. (2008), the Kwangsian gneissoid granites have A/CNK (molar $Al_2O_3/CaO + Na_2O + K_2O$) ranging from 1.02 to 1.36 and A/NK (molar $Al_2O_3/Na_2O + K_2O$) from 1.2 to 2.3 (Fig. 11a). CIPW-normative calculation gives 27–52 vol.% Qz, 8.1–33.4 vol.% Or, 9.2–28.2 vol.% Ab, 3.1–15.9 vol.% An and 1.0–9.5 vol.% corundum. Such characteristics are consistent with those of S-type granites. Our samples exhibit SiO_2 of 67.1–77.6 wt.%, $K_2O + Na_2O$ of 3.9–7.8 wt.%, Al_2O_3 of 10.2–15.4 wt.%, FeOt of 1.0–6.5 wt.%, MgO of 0.5–2.5 wt.%, TiO2 of 0.15–0.89 wt.% and P_2O_5 of 0.05–0.22 wt.%. They show generally $K_2O > Na_2O$ and have low CaO contents (0.6–3.2 wt.% and mostly lower than 1.8 wt.%) but high $TiO_2 + FeOt + MgO$ (2.6–8.7 wt.%) and $Al_2O_3/(Na_2O + CaO)$ ratios (2.2–3.3). In the QAF diagram (Fig. 11b), they plot in the fields of monzogranite and quartz-rich granite. In the Harker diagrams (Fig. 12a–g), these gneissoid granites generally exhibit negative correlations of Al_2O_3, MgO, CaO, MnO and FeOt with SiO_2, but insignificant correlations are shown between SiO_2 and $K_2O + Na_2O$ and TiO_2. P_2O_5 increases for the samples with SiO_2 contents of higher than ca. 72% but decreases with increasing SiO_2 for those with SiO_2 contents of less than ca. 72 wt.% (Fig. 12h). Rubidium, Zr, Sr, Ba and Eu decrease with increasing of SiO_2 for these samples. Rubidium, and Ba are more enriched relative to Sr, and Rb/Sr and Rb/Ba ratios vary from 0.52 to 2.73 and 0.11 to 0.67, respectively. The paragneissic enclaves in the Kwangsian gneissoid granites from the southern Wuyi and Yunkai Domains have SiO_2 of 62.5–72.3 wt.% and $TiO_2 + FeOt + MgO$ of 6.9–11.6 wt.%. These enclaves have higher FeOt, TiO_2, MgO but lower $K_2O + Na_2O$ and CaO than those of the gneissoid granites at comparable SiO_2 (Fig. 12a–g).

The gneissoid granites and paragneissic enclaves show similar Chondrite-normalized patterns of rare-earth elements (REE) despite their different abundances (Fig. 13a). The gneissoid granites exhibit total REE contents of 96–436 ppm, with $(La/Yb)n = 6.13–22.5$ and $(Gd/Yb)n = 1.05–2.94$ (Table 2). The paragneissic enclaves have total REE contents of 77–264 ppm, with $(La/Yb)n = 4.23–20.7$ and $(Gd/Yb)n = 0.73–3.48$. The size of their negative europium anomalies, expressed as Eu/Eu* ratios, is the range of 0.30–0.61 and 0.37–0.78, respectively (Table 2). On the primitive mantle-normalized spidergram (Fig. 13b), the gneissoid granites exhibit a pattern with strongly negative Ba, Sr, Nb, P and Ti anomalies and positive Pb anomalies, similar to those of the paragneissic enclaves. Such a pattern is also consistent with those of the Precambrian sedimentary rocks (Chen and Jahn, 1998; Shen et al., 1998; Wan et al., 2007, 2010) and Indosinian granites (Wang et al., 2007a) in the eastern SCB, as well as the Kwangsian gneissoid granites reported by Wan et al. (2010) and Zeng et al. (2008). As shown in Table 2, these gneissoid granites have initial $^{87}Sr/^{86}Sr$ ratios between 0.70924 and 0.72935 and $\varepsilon_{Nd}(t)$ values between −6.4 and −11.4, respectively, with Nd model ages of 1.6–2.2 Ga (Fig. 14a). The similar Sr–Nd isotopic compositions and Nd model ages ($^{87}Sr/^{86}Sr$ ratios of 0.71043–0.73468, $\varepsilon_{Nd}(t)$ value of −6.14 to −10.25 and Nd model ages of 1.6–2.2 Ga) are given by the paragneissic enclaves. Such isotopic compositions are consistent with those of the Precambrian metasedimentary rocks in the SCB (e.g., Shen et al., 1998; Wang et al., 2007a), also similar to those of the S-type granites and Ordovician sediments from the Lachlan Fold Belt in

Fig. 10. (a–g) Concordia diagrams of zircon U–Pb data for representative samples from the Yunkai Domain. (a) 09YK-8B orthogneiss (Yunlong, Xingyi); (b) 09YK-10A gneissoid granite (Jintong, Xinyi); (c) 09YK-12 orthogneiss (Licun, Rongxian); (d) 09YK-15a gneissoid granite (Shiwo, Beiliu); (e) 09YK-16 T leucosome in migmatite (Xieji, Gaozhou); (f) 09YK-17 orthogneiss (Xintong, Gaozhou); (g) 09YK-16 K paragneiss (Xieji, Gaozhou).

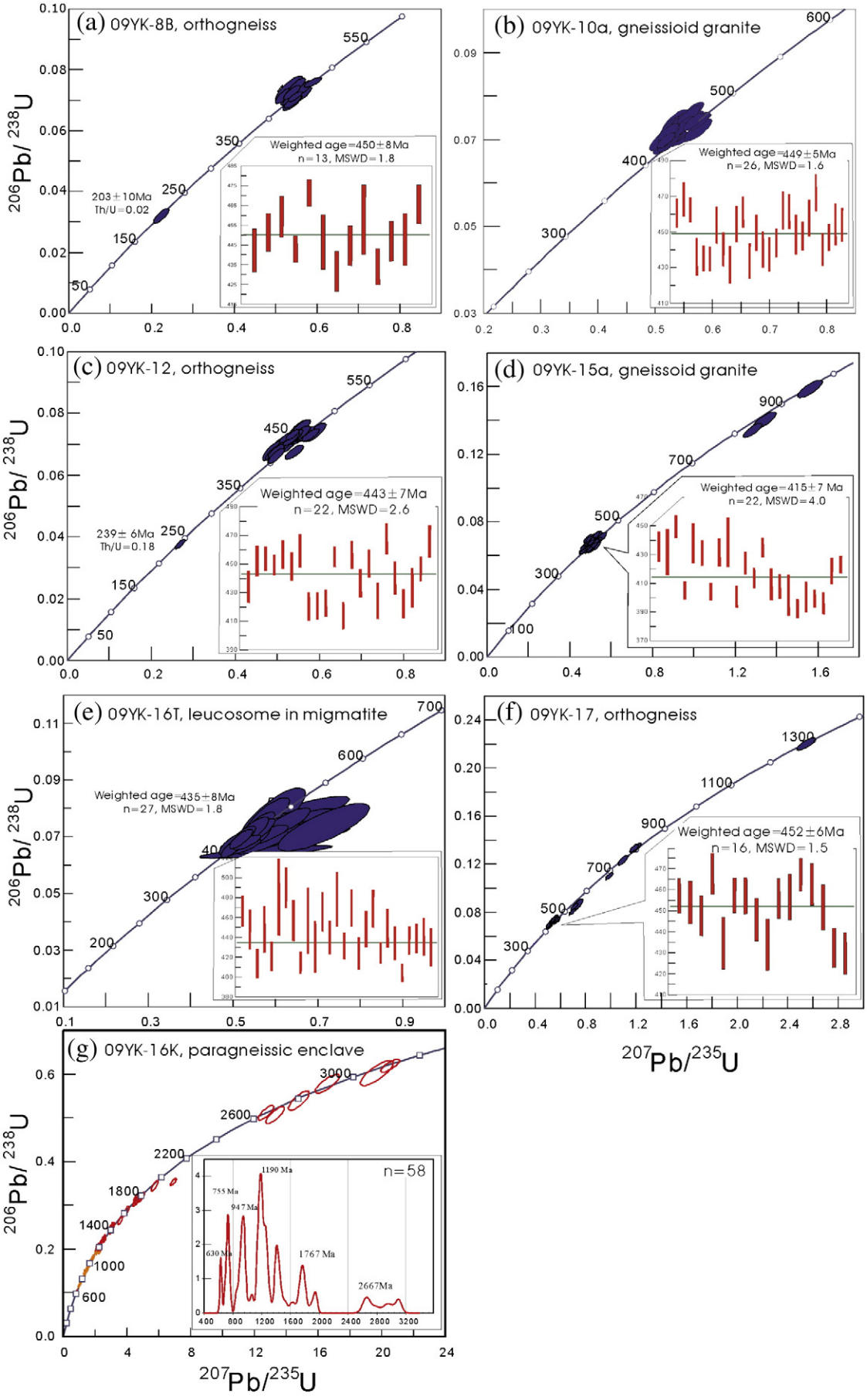
(a) 09YK-8B, orthogneiss
Weighted age=450±8Ma
n=13, MSWD=1.8
203±10Ma
Th/U=0.02
(b) 09YK-10a, gneissoid granite
Weighted age=449±5Ma
n=26, MSWD=1.6
(c) 09YK-12, orthogneiss
Weighted age=443±7Ma
n=22, MSWD=2.6
239± 6Ma
Th/U=0.18
(d) 09YK-15a, gneissoid granite
Weighted age=415±7 Ma
n=22, MSWD=4.0
(e) 09YK-16T, leucosome in migmatite
Weighted age=435±8Ma
n=27, MSWD=1.8
(f) 09YK-17, orthogneiss
Weighted age=452±6Ma
n=16, MSWD=1.5
(g) 09YK-16K, paragneissic enclave
n=58
1190 Ma
755 Ma
947 Ma
630 Ma
1767 Ma
2667Ma
206Pb/238U
207Pb/235U

Table 2
Elemental and Sr–Nd isotopic analyses for the Kwangsian gneissoid granites and paragneissic enclaves in the eastern South China Block.

Samples	Kwangsian gneissoid granite									
	09WG-03	09WG-4	09WG-07	09WG-12	09WG-25	08WY-6	09WG-57	09WG-32 g	09WG-32E	09WG-93
SiO_2	69.00	72.10	69.88	67.06	70.68	69.37	73.47	73.68	70.10	72.91
TiO_2	0.60	0.15	0.89	0.70	0.70	0.58	0.41	0.24	0.32	0.17
Al_2O_3	14.08	14.15	12.75	15.04	12.47	14.78	12.42	13.94	14.99	14.50
CaO	2.82	1.29	2.79	3.24	2.58	1.59	1.04	2.08	1.03	0.64
FeOt	4.53	1.23	5.26	4.46	5.82	3.35	2.96	1.46	2.14	1.03
MgO	1.80	1.26	2.53	1.98	0.81	1.19	1.17	1.76	2.01	1.86
K_2O	1.86	4.50	2.44	3.09	2.06	5.08	4.43	2.36	4.65	4.21
Na_2O	3.41	3.04	1.83	3.14	1.92	2.71	2.58	3.59	3.05	3.29
MnO	0.08	0.04	0.11	0.05	0.07	0.07	0.06	0.03	0.04	0.03
P_2O_5	0.15	0.07	0.16	0.22	0.16	0.19	0.06	0.11	0.10	0.05
LOI	1.15	1.90	1.25	1.03	2.62	1.23	1.29	0.84	0.93	0.67
Total	99.48	99.72	99.89	100.00	99.88	100.13	99.89	100.10	99.36	99.37
Sc	16.71	4.33	17.73	22.71	8.90	11.76	7.43	6.82	5.06	2.63
V	127.4	21.0	137.1	114.1	55.8	92.9	43.0	43.3	33.6	26.7
Cr	69.5	6.5	64.1	103.1	15.8	79.8	11.7	26.2	27.3	11.2
Co	16.91	2.18	21.21	19.25	7.96	15.86	6.06	7.71	5.44	3.12
Ni	33.3	2.3	36.4	48.4	6.5	38.7	7.3	13.0	12.3	14.9
Ga	25.93	16.68	25.29	23.08	21.21	16.30	19.71	15.11	17.99	15.68
Rb	106.8	194.9	105.7	150.8	132.3	116.4	224.3	178.9	184.7	150.6
Sr	92.41	80.45	177.30	65.54	253.50	89.47	129.90	113.30	136.50	130.80
Y	35.54	20.14	39.30	62.07	30.57	26.63	31.48	50.85	21.11	9.66
Zr	197	78	184	296	302	178	275	186	70	155
Nb	10.21	8.42	10.54	11.83	19.63	9.95	9.38	17.75	18.17	10.65
Cs	7.58	8.92	9.52	3.70	3.87	6.28	10.47	4.34	6.91	7.13
Ba	533	294	549	508	1013	446	833	526	567	624
La	32.78	19.19	29.87	89.91	78.56	31.97	28.75	34.35	35.16	23.22
Ce	69.17	38.22	62.81	187.60	152.80	63.57	57.23	69.41	67.87	44.79
Pr	8.91	4.66	8.05	21.64	17.30	7.72	6.70	8.35	7.84	5.09
Nd	35.15	16.16	30.47	77.04	62.40	28.53	24.95	29.87	27.67	17.67
Sm	7.18	3.51	6.31	14.42	10.52	5.56	5.15	6.52	5.42	3.45
Eu	1.54	0.55	1.39	1.41	1.93	1.10	1.13	1.04	1.06	1.05
Gd	6.88	3.31	6.08	13.02	8.39	5.38	5.57	6.80	4.64	2.68
Tb	1.09	0.55	1.02	1.88	1.30	0.81	0.97	1.22	0.74	0.40
Dy	6.29	3.38	6.54	10.78	6.44	4.75	5.85	7.87	4.13	2.02
Ho	1.35	0.69	1.47	2.37	1.16	0.97	1.23	1.73	0.74	0.34
Er	3.85	2.05	4.33	6.86	2.87	2.64	3.36	4.95	1.89	0.89
Tm	0.58	0.36	0.66	1.07	0.40	0.39	0.46	0.79	0.27	0.12
Yb	3.79	2.53	4.27	6.84	2.47	2.60	2.81	5.26	1.63	0.76
Lu	0.57	0.39	0.63	1.02	0.38	0.39	0.42	0.79	0.24	0.12
Hf	5.54	2.83	5.29	8.58	7.69	4.94	7.62	5.23	2.03	4.61
Ta	0.86	1.90	0.90	0.80	1.30	0.96	1.53	1.56	1.66	1.29
Pb	5.8	36.2	21.3	23.0	30.8	36.6	33.0	32.4	49.5	54.2
Th	10.05	10.25	9.51	45.85	25.74	12.93	22.55	17.48	16.78	11.84
U	4.62	5.10	2.06	2.97	2.08	2.77	4.80	3.56	3.31	3.36
$^{87}Rb/^{86}Sr$	3.3507	7.0237		6.6707	1.5131		5.0061	4.5778		3.3381
$^{147}Sm/^{144}Nd$	0.1235	0.1313		0.1132	0.1020		0.1249	0.1320		0.1182
$^{87}Sr/^{86}Sr$	0.729760	0.763572		0.751930	0.722052		0.747083	0.752898		0.735798
2 σ	0.000014	0.000017		0.000016	0.000021		0.000013	0.000014		0.000012
$^{143}Nd/^{144}Nd$	0.512090	0.511991		0.512074	0.511872		0.511852	0.511983		0.511920
2 σ	0.000008	0.000009		0.000007	0.000010		0.000011	0.000011		0.000008
$^{87}Sr/^{86}Sr(i)$	0.709238	0.720555		0.711074	0.712785		0.716422	0.724860		0.715353
εNd(t)	−6.67	−9.03		−6.41	−9.74		−11.40	−9.27		−9.70
$T_{DM}(Ga)$	1.80	2.15		1.64	1.75		2.23	2.18		1.97

LOI: Loss ion ignition, chondrite uniform reservoir values, $^{147}Sm/^{144}Nd = 0.1967$, $^{143}Nd/^{144}Nd = 0.512638$, are used for the calculation. $\varepsilon_{Nd}(t)$ is calculated by assuming 430 Ma for these samples. Sm, Nd, Rb, and Sr: ppm.

eastern Australia and the Indosinian granites in the eastern SCB (e.g., Healy et al., 2004; Wang et al., 2007a).

6. Discussion

6.1. Temporal and spatial pattern of the Kwangsian granites

Available data show that there are numerous massive granites with an exposure area over 20 000 km^2 in the eastern SCB (e.g., Shu et al., 2008a, 2008b; Zhou et al., 2006, 2007). The massive granites have peraluminous compositions and occur predominantly in the areas east of the Anhua–Luocheng Fault (Fig. 1). They were traditionally considered to be younger than the gneissoid granites (e.g., Hunan BGMR, 1988; Jiangxi BGMR, 1985; Zhou, 2003). The recently obtained age data show that these massive granites formed between 390 Ma and 458 Ma with a peak age at 428 Ma (Fig. 15a, e.g., Zeng and Liu, 2000; Xu et al., 2005; Zhang et al., 2010a, 2010b).

Our geochronological results for twenty-four gneissoid granites give zircon U–Pb ages of 424–456 Ma (Wugong), 410–457 Ma (Northern Wuyi), 426–438 Ma (Southern Wuyi) and 415–450 Ma (Yunkai), respectively (Table 1). The ages can be interpreted as the crystallization time of these granites. Recently SHRIMP and LA zircon U–Pb dating has also revealed the presence of the middle Paleozoic (Kwangsian) gneissoid granites in the Cathaysia Block (also see Figs. 5, 7 and 9; e.g., Charvet et al., 2010; Li et al., 2010c; Wan et al., 2007, 2010; Wang et al., 2007b; Yang et al., 2010; Zeng et al., 2008). For example, (1) some gneissoid granites and

09WG-94	09WG-96	08FJ-131B	08FJ-135	09WG-136	09YK-8B	09YK-10A	09YK-12	09YK-15A
70.67	76.98	77.60	75.93	72.61	73.80	75.77	72.66	73.02
0.56	0.63	0.62	0.51	0.65	0.69	0.66	0.64	0.62
14.24	11.00	10.63	10.17	12.19	11.92	11.08	12.79	11.92
1.77	1.31	1.26	0.93	1.81	1.65	1.53	1.87	1.91
4.20	2.47	2.19	3.60	5.32	4.77	4.17	4.57	5.06
1.53	1.32	1.03	1.33	0.82	0.75	0.68	0.50	0.83
2.49	2.56	2.52	2.76	2.42	2.44	2.40	3.10	2.10
2.83	1.95	1.99	2.40	2.00	1.84	1.51	1.36	2.17
0.04	0.04	0.04	0.07	0.06	0.05	0.04	0.04	0.05
0.12	0.14	0.15	0.12	0.15	0.15	0.15	0.13	0.13
1.38	1.18	1.65	1.92	1.30	1.28	1.29	1.71	1.54
99.84	99.59	99.69	99.75	99.33	99.32	99.30	99.36	99.36
13.31	8.25	8.09	8.05	10.28	10.07	8.91	11.38	10.67
70.2	52.5	51.0	59.4	64.1	60.7	51.5	69.1	63.0
69.6	56.6	53.2	47.2	69.0	62.0	38.5	72.6	68.9
9.58	9.53	8.22	18.19	11.82	9.12	7.88	11.50	11.15
25.6	21.6	20.1	30.2	27.3	23.4	18.9	27.7	26.3
18.37	13.23	13.26	13.61	16.47	15.08	13.26	16.63	15.59
112.5	82.7	85.1	62.8	114.3	105.3	86.5	130.7	103.5
125.20	91.23	102.20	81.87	107.80	107.80	83.63	83.07	120.80
32.15	27.71	27.80	18.43	27.20	26.35	21.53	25.87	26.57
288	288	284	167	274	300	109	212	244
12.97	11.82	12.00	8.16	13.06	13.25	12.81	12.67	12.38
3.06	2.95	2.59	3.54	8.37	6.90	5.16	7.66	6.99
455	779	730	136	528	624	661	775	572
39.82	43.01	45.16	21.72	46.64	49.87	53.37	43.49	42.42
77.76	84.64	88.16	44.68	93.20	98.49	102.50	85.07	83.35
9.52	10.19	10.42	5.37	11.13	11.80	12.25	10.35	10.01
34.53	35.58	36.26	19.38	39.73	41.45	43.62	36.87	35.64
6.80	6.54	6.55	3.80	7.06	7.36	7.67	6.73	6.55
1.44	1.17	1.16	0.88	1.35	1.44	1.17	1.18	1.31
6.32	6.14	5.93	3.78	6.22	6.33	6.51	6.18	6.22
0.97	0.89	0.86	0.60	0.90	0.91	0.87	0.88	0.87
5.53	4.93	4.82	3.35	5.01	4.85	4.33	4.89	4.80
1.10	0.97	0.93	0.64	0.97	0.96	0.76	0.94	0.93
3.37	2.77	2.62	1.76	2.73	2.62	1.99	2.58	2.63
0.58	0.42	0.39	0.26	0.40	0.40	0.29	0.39	0.38
4.42	2.76	2.64	1.70	2.69	2.57	1.79	2.52	2.62
0.71	0.40	0.40	0.25	0.40	0.39	0.27	0.38	0.38
7.81	7.62	7.53	4.44	7.49	8.17	2.44	6.07	6.48
1.49	1.06	1.09	0.77	1.17	1.19	1.18	1.16	1.09
19.7	9.7	13.2	16.5	33.1	24.9	22.0	25.7	24.2
17.17	19.13	19.03	8.27	19.34	21.05	23.09	18.51	19.09
4.20	3.45	3.36	1.31	3.59	3.83	3.69	3.46	3.46
	2.6281	2.4130	2.2221	3.0740	2.8320	2.9973	4.5615	2.4840
	0.1112	0.1093	0.1186	0.1074	0.1074	0.1063	0.1105	0.1111
	0.745443	0.725832	0.728944	0.731661	0.727836	0.728705	0.742383	0.724573
	0.000016	0.000013	0.000022	0.000013	0.000014	0.000022	0.000015	0.000013
	0.511842	0.511914	0.511832	0.511837	0.511832	0.511996	0.511947	0.512004
	0.000013	0.000011	0.000013	0.000007	0.000008	0.000011	0.000007	0.000009
	0.729346	0.711053	0.715334	0.712834	0.710491	0.710347	0.714445	0.709359
	−10.83	−9.33	−12.20	−10.73	−10.83	−7.56	−8.75	−7.67
	1.95	1.81	2.18	1.89	1.90	1.74	1.78	1.71

(*continued on next page*)

leucosomes from the Wuyi Domain yield zircon U–Pb ages of 410–458 Ma (Charvet et al., 2010; Li et al., 2010b, 2010c; Wan et al., 2007, 2010; Zeng et al., 2008; Zeng and Liu, 2000). (2) The zircon U–Pb ages of 439–454 Ma and 413–467 Ma are given by gneissoid granites from the Baiyun and Yunkai Domains (e.g., Wan et al., 2007, 2010; Wang et al., 2007b; Yang et al., 2010). The synthesis of these geochronological data for the gneissoid granites indicates the crystallization age of 410–457 Ma with an age peak at 436 Ma (Fig. 15b), generally similar to that of the massive granites in the eastern SCB (Fig. 15a). The gneissoid granites are extensively exposed in the Wugong and Wuyi–Baiyun–Yunkai Domains in the Cathaysia interior, whereas the massive granites predominantly occur in the areas in the eastern SCB east of the Anhua–Luocheng Fault (Fig. 1).

As mentioned above, almost all of these samples were collected from the so-called Precambrian metamorphic rocks that were previously mapped as the components of the Badu, Mayuan, Yunkai, Zhoutan and Taoxi "Groups" of the Cathaysia Block (e.g., Fujian BGMR, 1985; Guangdong BGMR, 1988; Jiangxi BGMR, 1984; Li et al., 2010c; Zhejiang BGMR, 1996). Our results show that many metaigneous rocks previously mapped as the Precambrian gneiss and migmatite are actually the Kwangsian anatectic granites in the Wugong and Wuyi–Yunkai Domains. Therefore, the Precambrian basement in the Cathaysia Block is not so widely distributed as previously thought (e.g., Fujian BGMR, 1985; Guangdong BGMR, 1988; Guangxi BGMR, 1985). In combination with other geochronological data (e.g., Li, 1997; Li et al., 2010c; Wan et al., 2007, 2010; Xiang et al., 2008; Yu et al., 2009, 2010), it

Table 2 (*continued*)

Samples	Kwangsian gneissoid granite		Paragneissic enclave in the Kwangsian gneissoid granite								
	09YK-16 T	09YK-17	09WG-32H	09WG-32A1	09WG-32A2	09WG-32A3	09YK-16 N	09YK-16 K	09YK-16 L	09WG-32B	09WG-32E
SiO_2	72.86	67.31	68.24	64.00	71.86	71.49	67.53	67.17	70.14	72.30	62.46
TiO_2	0.62	0.65	0.98	0.91	0.69	0.74	0.80	0.76	0.52	0.74	0.94
Al_2O_3	13.02	14.54	13.78	16.48	14.50	13.99	14.06	13.69	13.66	14.18	17.55
CaO	1.84	2.32	2.33	2.39	1.64	1.91	0.99	1.31	1.30	2.24	1.13
FeOt	4.53	6.54	8.18	8.02	4.35	5.03	8.21	6.78	7.08	4.29	7.84
MgO	0.46	0.47	1.23	1.57	1.85	2.02	2.63	2.40	2.41	1.77	2.79
K_2O	2.87	4.05	2.91	2.81	1.32	1.54	3.38	2.69	2.96	1.27	3.13
Na_2O	2.26	1.06	1.15	2.11	2.87	1.78	0.93	1.14	1.09	1.55	1.97
MnO	0.04	0.05	0.12	0.11	0.05	0.07	0.22	0.11	0.18	0.11	0.19
P_2O_5	0.13	0.13	0.06	0.17	0.13	0.13	0.06	0.05	0.05	0.09	0.21
LOI	1.36	2.25	0.85	1.32	0.64	0.89	1.00	3.78	0.62	1.26	1.67
Total	99.98	99.36	99.83	99.89	99.90	99.61	99.81	99.87	100.01	99.79	99.87
Sc	10.84	13.81	3.26	11.97	10.80	11.80	24.54	12.60	23.49	11.13	9.60
V	65.1	88.2	28.0	102.0	85.8	97.2	135.8	162.0	132.0	84.7	70.5
Cr	69.9	87.5	12.3	76.5	75.3	74.9	107.8	97.4	93.8	62.5	52.7
Co	11.26	13.85	3.86	14.59	13.29	14.37	21.65	16.70	16.98	11.76	10.40
Ni	28.0	34.4	8.1	34.9	27.9	31.3	51.8	43.8	42.7	26.4	21.4
Ga	15.68	20.24	16.13	15.25	20.58	17.08	20.45	22.78	20.59	14.94	21.66
Rb	130.4	182.7	104.1	201.1	162.7	164.0	168.3	151.1	150.7	122.2	152.3
Sr	80.86	66.85	122.70	97.55	89.11	89.92	65.42	70.37	67.55	138.90	131.90
Y	24.00	29.43	13.06	23.35	14.80	29.97	83.68	32.48	72.66	31.69	19.74
Zr	219	204	190	212	53	207	315	278	277	197	136
Nb	12.26	13.28	8.50	14.77	14.12	16.19	13.12	11.25	11.69	14.05	12.01
Cs	7.83	19.26	4.57	10.29	11.00	11.57	3.78	4.20	3.94	8.59	8.88
Ba	733	844	215	173	82	104	710	504	567	308	95
La	40.63	48.53	16.81	33.01	31.54	33.07	52.85	48.35	52.27	27.30	22.71
Ce	79.97	92.90	32.42	67.38	65.89	66.30	102.10	95.99	104.90	55.20	44.65
Pr	9.66	11.33	3.62	7.98	7.77	8.17	12.17	11.29	12.65	6.80	5.26
Nd	33.96	40.42	12.80	30.17	28.77	30.11	42.57	40.51	43.95	25.67	18.99
Sm	6.27	7.39	2.65	5.54	5.59	5.81	7.87	7.43	8.33	5.00	4.11
Eu	1.08	1.42	0.84	0.79	0.66	0.74	1.24	1.21	1.20	1.32	0.75
Gd	5.39	6.66	2.21	4.85	4.63	5.29	8.00	6.69	8.20	4.89	3.76
Tb	0.81	0.99	0.37	0.74	0.69	0.87	1.54	1.02	1.50	0.87	0.64
Dy	4.42	5.53	2.18	4.21	3.29	5.15	12.03	5.86	10.74	5.56	3.63
Ho	0.88	1.07	0.43	0.85	0.53	1.05	3.14	1.20	2.71	1.11	0.69
Er	2.34	3.00	1.22	2.40	1.27	2.91	9.57	3.21	7.92	3.07	1.83
Tm	0.34	0.44	0.18	0.37	0.18	0.46	1.42	0.43	1.14	0.48	0.27
Yb	2.34	2.97	1.14	2.49	1.08	2.96	8.86	2.54	7.05	3.14	1.62
Lu	0.35	0.44	0.17	0.39	0.16	0.47	1.14	0.35	0.95	0.49	0.25
Hf	5.86	6.11	5.43	5.43	1.48	5.47	9.33	8.12	7.49	5.14	3.77
Ta	1.10	1.26	1.19	1.18	1.12	1.46	0.92	0.92	0.88	1.15	1.87
Pb	25.7	26.3	31.5	8.4	15.2	12.4	26.8	21.6	23.9	14.4	19.3
Th	17.28	20.90	8.92	11.27	13.17	11.65	25.75	22.73	25.52	9.01	9.03
U	3.15	3.96	3.21	2.59	2.66	2.92	2.34	1.92	2.14	2.29	1.67
$^{87}Rb/^{86}Sr$			2.4597	5.9767		5.2877		6.2252	6.4679	2.5506	3.3476
$^{147}Sm/^{144}Nd$			0.1250	0.1110		0.1167		0.1109	0.1147	0.1179	0.1310
$^{87}Sr/^{86}Sr$			0.725492	0.771284		0.748366		0.752853	0.753042	0.732844	0.732436
2 σ			0.000012	0.0002		0.000017		0.000019	0.000012	0.000022	0.000021
$^{143}Nd/^{144}Nd$			0.511988	0.511872		0.511896		0.511947	0.512092	0.511960	0.511957
2 σ			0.000010	0.000007		0.000009		0.000008	0.000010	0.000007	0.000009
$^{87}Sr/^{86}Sr(i)$			0.710427	0.734678		0.715980		0.714725	0.713428	0.717222	0.711933
εNd(t)			−8.75	−10.25		−10.09		−8.78	−6.14	−8.90	−9.69
$T_{DM}(Ga)$			2.00	1.90		1.98		1.79	1.63	2.15	2.20

is inferred that these groups of the eastern SCB have abundant components with crystallization ages ranging from 410 Ma to 1870 Ma. The original stratigraphic terminology of "Group" in the eastern SCB should be abandoned, as proposed by Wan et al. (2007, 2010). The term "Complex" is more suitable for describing the "Group" in the Cathaysia Block (Li et al., 2010c).

6.2. Petrogenetic constraints

The gneissoid granites are peraluminous granites with almost all of them showing a strongly peraluminous signature, suggesting their petrogenesis probably being related to (1) fractionation of aluminous-poor magma (Zen, 1986), or (2) partial melting of metasedimentary and/or meta-igneous sources. Fractional crystallization of the magma and removal of plagioclase, K-feldspar, biotite and apatite are certainly important for the formation of the gneissoid granites, as suggested by decreasing of FeOt, MgO, Al_2O_3, MnO, Sr and Ba with increasing SiO_2. The increasing Rb/Sr ratios with decreasing Sr, together with a significant depletion in Sr, Ba and Eu in Fig. 13b, further supports that plagioclase and K-feldspar have been removed during the magma evolution. The negative P and Ti anomalies indicate the fractionation of apatite and Fe–Ti oxides. The fractionation of aluminous-poor magma usually generates metaluminous, Na-rich rocks rather than peraluminous, K-rich rocks in a closed system (e.g., Gaudemer et al., 1988; Zen, 1986). In addition, extensive clinopyroxene and feldspar fractionation would result in a significant increase in Ca/Al ratios and a decrease in Eu/Eu*

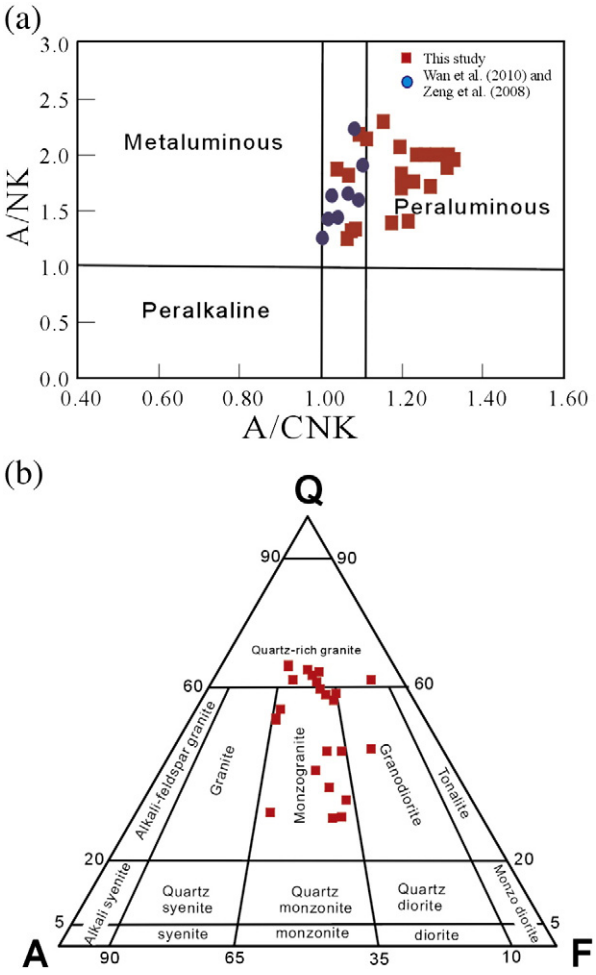

Fig. 11. (a) QAF diagram for the Kwangsian gneissoid granites from the eastern South China Block.

values of the evolved melt, respectively, in contrary to our observations. Such characteristics, together with the wide variation in whole-rock Sr–Nd and zircon Hf isotopic compositions for these samples, cannot be interpreted by the petrogenetic model of a simple closed-system fractionation.

Zircon is one of the earliest crystallization minerals. It retains its original isotopic composition and thus can be used to trace petrogenetic process (e.g., Griffin et al., 2002). The zircons crystallized in the Kwangsian gneissoid granites gave εHf(t) values ranging from +2.4 to −19.4 (n = 552) with a peak at −4 (almost all grains varying from −1 to −12). They fall into the field between the lines of evolved Archean crust and Neoproterozoic depleted mantle (Fig. 16a). The corresponding Hf model ages vary from 1.1 Ga to 2.2 Ga with the peak at 1.40 Ga, similar to their Nd model ages 1.7–2.5 Ga for these gneissoid granites (e.g., Wan et al., 2007, 2010; Yu et al., 2009, 2010). Such model ages are consistent with the formation ages of the Cathaysia basement, but significantly older than the Kwangsian U–Pb formational ages of these grains (Fig. 16b). In the plot of εNd(t) and εHf(t) (Fig. 14b), these grains crystallized in the Kwangsian granites fall in the fields of the global lower crust and global sediments (e.g., Dobosi et al., 2003). In addition, the grains of them with the highest εHf(t) values are not from the gneissoid sample with highest εNd(t) values (inset in Fig. 14b).

In our analyzed samples, there are abundant Neoproterozoic (~750–1100 Ma) inherited grains (Supplementary Dataset 2 and Figs. 2–10). These inherited zircons show similar εHf(t) values (−15.3 to +12.6) to those of detrital zircons from the paragneissic enclaves (Supplementary Dataset 2 and Fig. 16a). Some of these grains give Hf model ages similar to their crystallization ages and show positive εHf(t) values of higher than +5 (Fig. 16a–b). These signatures suggest that significant input of juvenile crust or reworking of crustal materials shortly after its formation occur during Neoproterozoic rather than middle Paleozoic (Kwangsian) period. Available data show that the mantle-derived rocks have poorly occurred in the eastern SCB during Ordovician and Silurian time (420–480 Ma; e.g., Shu et al., 2008a, 2008b; Wang et al., 2010), also indicating minor involvement of basaltic magmas and insignificant lithospheric delamination during the Kwangsian period in the eastern SCB. Exposed in the Wuyi–Yunkai Domains are abundant high-grade metamorphic rocks with ages of the peak metamorphism and subsequent cooling being at 425–460 Ma and ~420 Ma, respectively (Yu et al., 2005; Li et al., 2010b, 2010c; Faure et al., 2009). The metamorphism of these rocks is characterized by a clockwise pressure–temperature path (Yu et al., 2003, 2005, 2007b; Zhao and Cawood, 1999), indicative of the Kwangsian orogenic regime with crustal thickening followed by exhumation/uplift (e.g., Li et al., 2010c). In such a convergent regime, it might be difficult for large-scale lithospheric extension to induce underplating of the juvenile basaltic magma. Thus the synthesis of these data indicates that the Kwangsian gneissoid granites have dominantly originated from Proterozoic crustal materials. The involvement of the Kwangsian juvenile component is rare. In addition, some Sinian–Cambrian recycled sediments also might contribute to the petrogenesis of the Kwangsian granite since the inherited grains of 510–644 Ma with strongly negative εHf(t) values are observed in the 09WG-4, -7, -25, -94, and 08FJ-131B and -135 samples (Supplementary Datasets 1 and 2).

A granite from a crustal metabasaltic source is generally characterized by high CaO/Na_2O and CaO/(MgO + FeOt) ratios but low Al_2O_3/TiO_2, Al_2O_3/(MgO + FeOt) and Rb/Ba ratios (e.g., Altherr et al., 2000; Anthony, 2005; Chappell and White, 1992; Jung et al., 2000; Patiño-Douce and Harris, 1998; Sylvester, 1998; Wang et al., 2007a). The majority of our samples exhibits relatively high FeOt, TiO_2 and CaO/Na_2O ratio and low Al_2O_3/(MgO + FeOt) (<2.50) and Rb/Sr ratios, suggesting the addition of the metabasaltic component in the source. This is further supported by the occurrence of abundant Precambrian amphibolite enclaves within the Kwangsian gneissoid granite in the Wuyi (e.g., Nanfeng and Taoxi) and Yunkai (e.g., Rongxian and Xinyi) Domains (e.g., Fujian BGMR, 1985; Guangxi BGMR, 1985; Qin et al., 2006). A question remains as to whether the Precambrian amphibolite is a sole source component for these gneissoid granites. Available data show that these migmatised amphibolites from the Wuyi and Yunkai Domains have lower $^{87}Sr/^{86}Sr$ ratios and higher εNd(t) values than those of the Kwangsian gneissoid granites (Li et al., 2005 and authors' unpublished data). Zircons from the migmatised amphibolites (northern Wuyi) have $\varepsilon Hf_{(430\ Ma)}$ values of −8.5 to +3.6 (e.g., Li et al., 2010b; Xiang et al., 2008), generally higher than those from the Kwangsian gneissoid granites. Such elemental and isotopic variations cannot only be interpreted by partial melting of Precambrian amphibolite.

The gneissoid granite samples are peraluminous with almost being strongly peraluminous. They show high initial $^{87}Sr/^{86}Sr$ ratios (0.70924–0.72935) and negative εNd(t) values (−6.4 to −11.4), similar to those of the paragneissic enclaves, also identical to those of the Precambrian migmatite, schist and paragneiss in the Wuyi Domain (e.g., Wan et al., 2007, 2010; Zeng et al., 2008). Such Sr–Nd isotopic compositions fall into the fields of Ordovician sedimentary rocks and S-type granites from the Lachlan Fold Belt (Fig. 13a; Healy et al., 2004; Wang et al., 2007a). They also show similar REE and incompatible elemental patterns with the paragneissic enclaves in the eastern SCB (Fig. 9a–b). Thus the metapelitic rock should be another necessary (even main) source for these gneissoid granites. Experimental studies also indicate that peraluminous melts might be sourced from an aluminous-rich pelitic component at 0.1–1.0 GPa (e.g., Miller, 1995; Patiño-Douce et al., 1990; Zen, 1986). This is further supported by the fact that the $\varepsilon Hf_{(430Ma)}$ values (−13.3 to +2.4) and Hf model ages of zircons from pelitic granulite and migmatite in the Wuyi Domain (e.g., Yu et al., 2005; Zeng et al., 2008) are similar to those of the Kwangsian gneissoid granites.

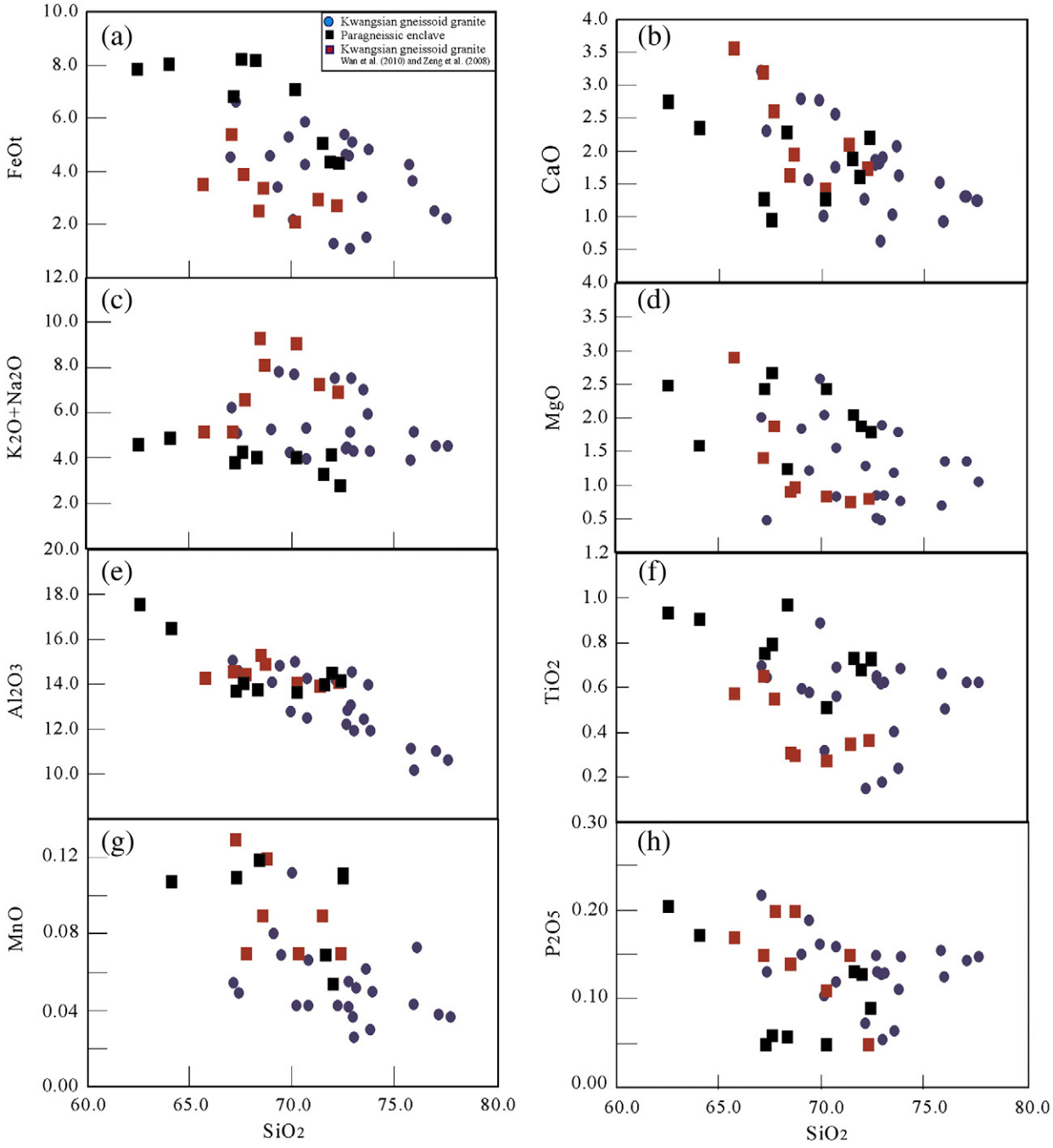

Fig. 12. SiO_2 versus (a) FeOt; (b) CaO; (c) $K_2O + Na_2O$; (d) MgO; (e) Al_2O_3; (f) TiO_2 for the Kwangsian gneissoid granites in the eastern South China Block. Symbols in (b–f) are the same as those in Fig. 12a.

In the CaO/Na_2O versus Al_2O_3/TiO_2 diagram (Fig. 17a), the gneissoid granites plot on the mixing line between metapelite- and metabasaltic-derived melts. In the plot of Rb/Sr and Rb/Ba ratios (Fig. 17b), they fall in the field of the plagioclase-rich and clay-poor source and mostly in that of Northern Himalayas granite in Fig. 17c. Thus, metapelitic and metabasaltic components should be involved in the source of these granites, which is also supported by their linear correlation as shown in Fig. 17d–e. One end-member is characterized by the metapelitic-derived melt. The other is most likely characterized by the metabasaltic-derived melt with low SiO_2, $^{87}Sr/^{86}Sr$ and Rb/Sr but high $FeO + MgO + TiO_2$ and εNd(t) values (Figs. 12, 14a and 17a–e). As a result, the Kwangsian gneissoid granites in the eastern SCB have been derived from an ancient metapelitic and metabasaltic source with minor inputs of newly underplating mantle-derived magmas.

6.3. Tectonic implications

The early Paleozoic tectonic regime between the Yangtze and Cathaysia Blocks is poorly constrained. Some authors invoke a Huanan oceanic crust between the two blocks being subducted during the Kwangsian period, leading to final closure of the so-called Hunan Ocean and collision of the Yangtze and Cathaysia Blocks (Chen et al., 2006; Guo et al., 1989; Ma et al., 2004; Shui, 1987; Xu et al., 1996). Others suggest that the Kwangsian orogeny represented intracontinental collision/remobilization in which the Yangtze and Cathaysia Blocks remained contiguous during early Paleozoic time (e.g., Charvet et al., 1996, 1999, 2010; Chen et al., 2000; Li et al., 2010b; Wang et al., 2007b, 2010). Our data show that the Kwangsian gneissoid granite and synchronous massive granite occur in the eastern SCB with a

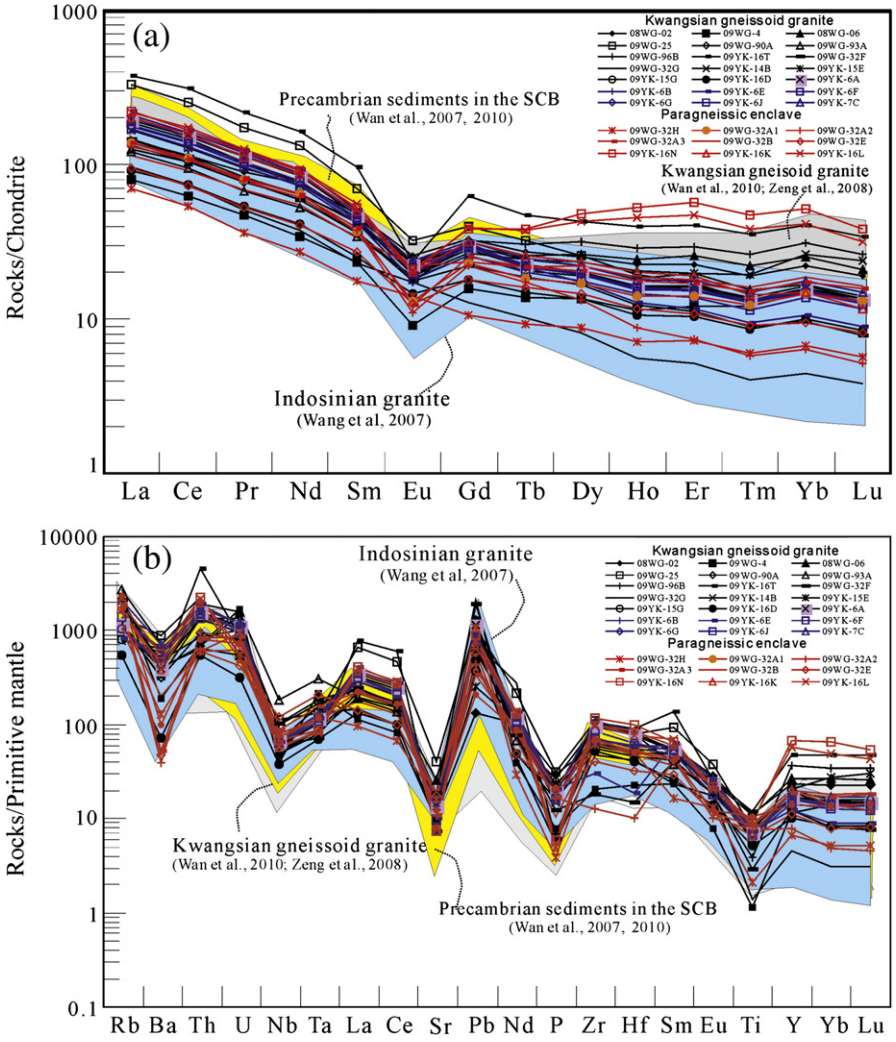

Fig. 13. (a) Chondrite-normalized REE and (b) primitive mantle-normalized incompatible elemental patterns for the Kwangsian gneissoid granites and paragneissic enclaves in the eastern South China Block. Normalized values for chondrite and primitive mantle are from Taylor and McLennan (1985) and Sun and McDonough (1989), respectively. Also shown are the patterns for Indosinian granite (Wang et al., 2007a), Kwangsian gneissoid granite reported by Wan et al. (2007) and Zeng et al. (2008) and Precambrian sediments (Wan et al., 2007, 2010) in the eastern South China Block.

planar distribution. Their occurrence is across the Jiangshan–Shaoxing fault that is considered to represent the suture of the consumed Huanan ocean in the subduction model (Ma et al., 2004; Shui, 1987; Wang et al., 2003, 2008; Xu et al., 1996; Zhang and Wang, 2007). As mentioned above, they are peraluminous rocks and largely originated from a Proterozoic metasedimentary source with poor inputs of juvenile component. The contemporaneous A-type granites and alkaline rocks are not observed in the eastern SCB. Also, it is absent for the early Paleozoic ophiolitic suites, calc-alkaline volcanic rocks and arc andesites that are associated with the closure of the proposed Huanan ocean (e.g., Fujian BGMR, 1985; Hunan BGMR, 1988; Jiangxi BGMR, 1984; Shu et al., 2008a, 2008b; Wang et al., 2010). Such observations are in contradiction with what would be expected for the proposed subduction model. The following sedimentary signatures further argue for an intracontinental tectonic regime rather than the independent development of the Yangtze and Cathaysia Blocks during early Paleozoic time. (1) There was linked and continuous biostratigraphical and paleoecological evolution from the Yangtze to Cathaysia Blocks (e.g., Chen et al., 2000; Liu and Xu, 1994; Rong et al., 2002, 2007). (2) The lower Paleozoic strata exhibit a transition from a slope/neritic siliciclastic, through an interstratified carbonate-siliciclastic, to a shallow-water carbonate-dominated succession from the Cathaysia to eastern and central Yangtze (e.g., Li et al., 2010a; Wang et al., 2010). (3) Over 900 detrital zircon grains from lower Paleozoic sandstones in the Yangtze and Cathaysia Blocks give similar patterns with age spectra clustering at ~2560 Ma, ~1850 Ma, ~1000 Ma and 890–760 Ma (Wang et al., 2010).

As mentioned above, the basement of the eastern SCB consists mainly of Proterozoic schist, gneiss, migmatite and amphibolite (e.g., Liu et al., 2008; Yu et al., 2009, 2010). The metamorphic grade generally shows a lowering trend from amphibolite-facies in the Cathaysia to greenschist-facies in the eastern Yangtze (e.g., Fujian BGMR, 1985; Zhejiang BGMR, 1996). The upper amphibolite- and granulite-facies metamorphic rocks only crop out in the Wuyi-Yunkai Domains (Fig. 1; e.g., Yu et al., 2005; 2007b), with their protoliths being similar to the source component of the Kwangsian gneissoid granites (Li et al., 2010b, 2010c; Wan et al., 2007, 2010; Yu et al., 2005; Yu et al., 2007a, 2007b). Recent zircon U–Pb dating results have demonstrated that the migmatised amphibolites and granulite-facies pelites along the Wuyi Domain were metamorphosed at 423–460 Ma with a peak at 435 Ma (e.g., Charvet et al., 2010; Li et al., 2010b, 2010c; Yu et al., 2005, 2007b). Our data (Table 1) also give metamorphic ages of 428 ± 3 Ma (07HJ-61), 454 ± 11 Ma (09WG-32f) and 453 ± 11 Ma (09WG-32e) from the Wugong and northern Wuyi

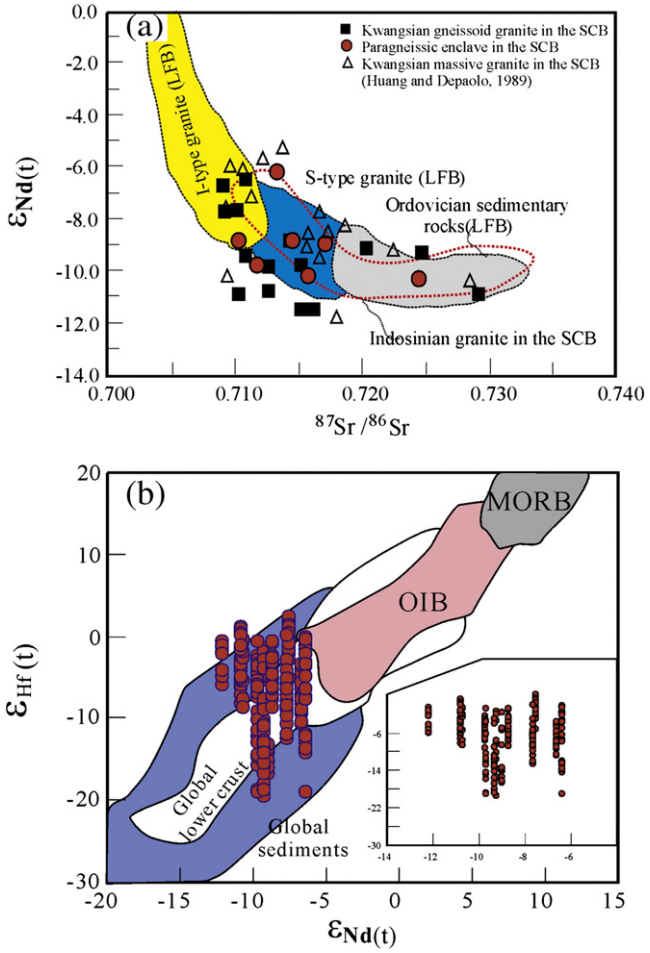

Fig. 14. (a) Initial Sr–Nd isotopic composition of the Kwangsian gneissoid granites and paragneissic enclaves in the eastern South China Block. (b) εNd(t) versus εHf(t) for the Kwangsian gneissoid granites in the eastern South China Block. Also shown in (a) are those for the Ordovician sedimentary rocks, S- and I-type granites from the Lachlan Fold Belt are from Healy et al. (2004). The data for the Indosinian and Kwangsian massive granites in (a) are from Wang et al. (2007a, 2007b) and Huang and Depaolo (1989), respectively.

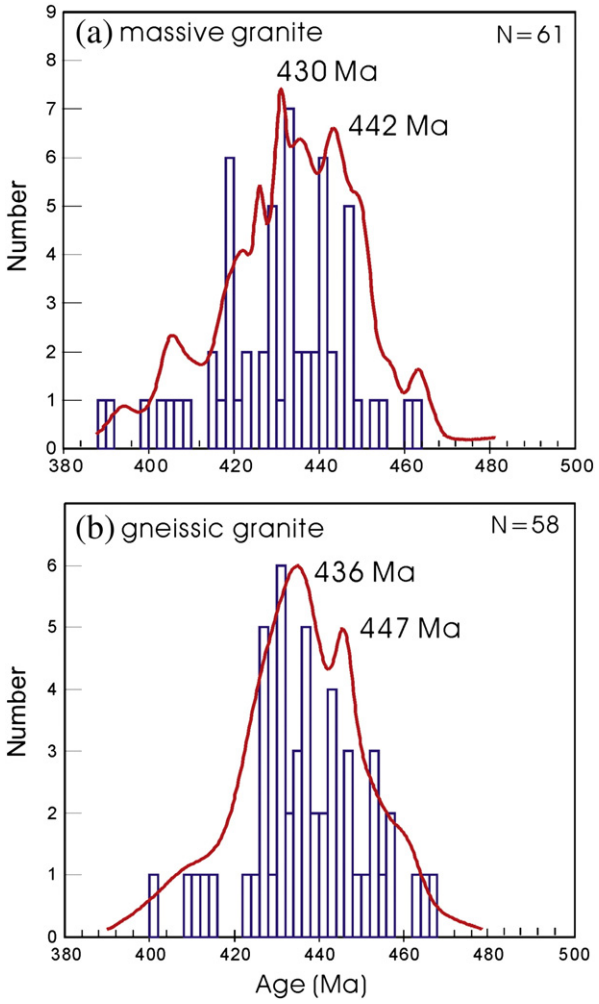

Fig. 15. Frequency of zircon U–Pb ages for the Kwangsian (a) massive granites and (b) gneissoid granites in the eastern South China Block. Data are from Faure et al. (1996), Huang and Depaolo (1989), Zeng and Liu (2000), Wu and Zhang (2003), Ding et al. (2005), Sun (2006), Wang et al. (2007b), Shu et al. (2008a, 2008b), Zeng et al. (2008), Chen et al. (2008), Wan et al. (2007, 2010), Xiang et al. (2008), Yang et al. (2010), Li et al. (2010c), Zhang et al. (2010b; 2011), Zhang et al. (2010a) and authors' unpublished data.

Domains. This indicates a good agreement of the temporal and spatial pattern as well as protolith materials between the Kwangsian gneissoid granite and high-grade metamorphic rocks. In the Shanzhaung, Doushui and Nandou areas in eastern SCB, the Kwangsian granites with crystallization ages of 400–430 Ma are directly overlain by the lower/middle Devonian sandstones, reflecting a rapid denudation at this time. Li et al. (2010c) obtained $^{40}Ar/^{39}Ar$ ages of 420–426 Ma for hornblende, biotite and muscovite from the Chencai and Wannian Complexes, suggestive of rapid cooling to 300–500 °C at ca 425 Ma. Thus the Kwangsian intracontinental structures of the Yangtze and Cathaysia Blocks were probably linked to doubly crustal thickening at ca. 460–423 Ma followed by rapid exhumation/orogenic collapse at ca. 425–400 Ma (e.g., Li et al., 2010c; Zhao and Cawood, 1999). The metamorphic ages of 423–460 Ma are considered to represent the time of the continental crust being tectonically thickened to reach the condition of peak metamorphism. Zhao and Cawood (1999) and Yu et al. (2003, 2005, 2007) revealed a clockwise, near-isothermal decompressional P–T path with peak metamorphism of T = 750–880 °C and P = 10–11 kbar on basis of the mineral assemblages and metamorphic reactions for the metamorphic rocks of the Cathaysia Block (also see Li et al., 2010c). Experimental studies have shown that mica and amphibole might start to breakdown at >700 °C (~5 kbar) and ~850 °C (P = 10 kbar) (e.g., Beard and Lofgren, 1991; Patiño-Douce and Harris, 1998; Rapp and Watson, 1995; Rushmer, 1991; Tompson, 1996; Vielzeuf and Schmidt, 2001; Wolf and Wyllie, 1991). Epidote and zoisite will be breakdown at approximately 750–800 °C at ~10 kbar (Lambert and Wyllie, 1972; Miller, 1995; Patiño-Douce et al., 1990; Vielzeuf and Schmidt, 2001; Zen, 1986). Thus the major minerals in the protolith materials can breakdown under the above-mentioned P–T conditions of metamorphism. The formation of these gneissoid granites might be closely related to the Kwangsian metamorphism of the Proterozoic basement materials in the eastern SCB. These observations, together with the above-mentioned petrogenetic discussion and other published data, allow us to propose the following scenario for the evolution of the Kwangsian orogenic event.

At ~460–425 Ma, the Neoproterozoic-early Paleozoic "Nanhua" failed rift between the Xuefeng and Wuyi–Yunkai Domains evidenced by the sedimentary and geochemical signatures (further data see in Wang and Li, 2003; Wang et al., 2010) was inverted to be a foreland-like compressive basin. The strong thrusting in the eastern SCB might have induced doubly crustal thickening (e.g., Charvet et al., 1996, 1999, 2010; Shu et al., 1991, 2008a, 2008b). This process resulted into the siliciclastics and igneous rocks to be doubly thickened and the amphibolite- to granulite-facies metamorphism and pervasive shearing deformation of these rocks in the

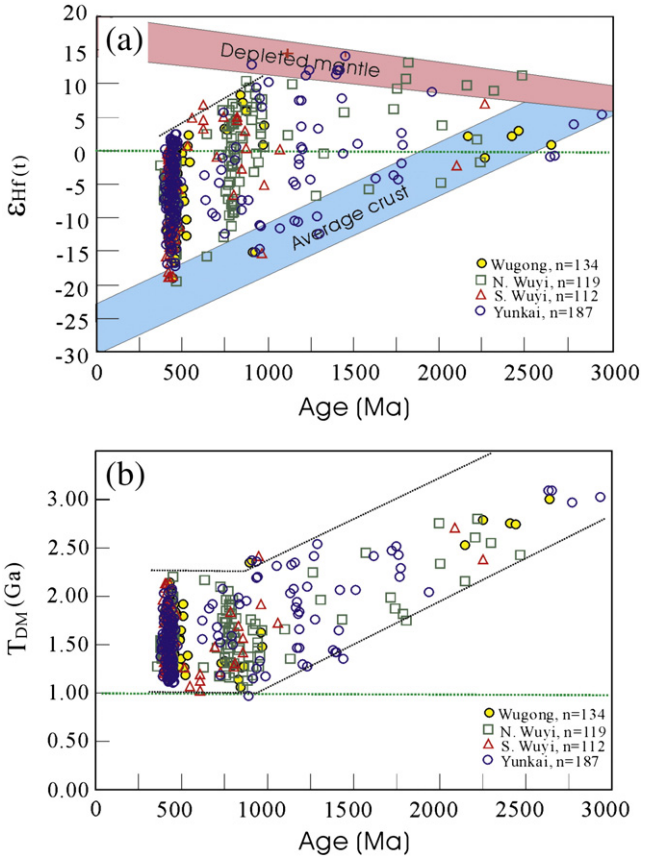

Fig. 16. Age (Ma) versus (a) εHf(t) and (b) T_{DM}(Hf) for zircons separated from the Kwangsian gneissoid granites and paragneissic enclaves from the Wugong, northern and southern Wuyi and Yunkai Domains in the eastern South China Block.

Wuyi–Yunkai Domains, as what happened in the Himalayas and Scandinavian Caledonides (e.g., Labrousse et al., 2010 and references therein). Progressive heating of buried materials induced the breakdown of hydrous minerals (e.g. mica) to generate initial melts (e.g., Harrison et al., 1999; Huerta et al., 1999; Streule et al., 2010). Once the melting of the source rocks had begun, effective viscosity of the middle crust was rapidly lowered and the mechanical strength was significantly softened, promoting the melt of the crustal materials at the deep level (Culshaw et al., 2010; Gerbi et al., 2010; Schilling et al., 1997; Streule et al., 2010). This pervasive flow under the compressional regime might result into a strong magmatic orientation, which can explain the formation of transposed gneissoid textures for these granites in the domains. At ~430–390 Ma, the increase of thermal weakening of the crust led to the gravity-derived flow in response to the orogenic collapse of the thickened crust, which was strongly coupled to rapid denudation of the thickened crust. The significantly promoted proportion of the melt would move along a path of isothermal decompression (Rosenberg and Handy, 2005; Rutter and Mecklenburgh, 2006; Vanderhaeghe and Teyssier, 2001; Wang et al., 2007a, 2007b) to generate voluminous 430–390 Ma granites in the eastern SCB.

It remains controversial as to the dynamic mechanism of this intracontinental orogen between the Yangtze and Cathaysia Blocks during Kwangsian (490–400 Ma) period. Wang et al. (2007b) proposed that this orogen might be linked to the subduction/collision between the SCB and North China Block. However, the majority of the Kwangsian high-grade metamorphic rocks and gneissic granites occur along the Wuyi–Yunkai Domains rather than on the northern margin of the Yangtze Block or along the Jiangshan–Shaoxing Fault at which the proposed Hunan Ocean was consumed. We note that, contemporaneous with the Kwangsian orogenic event in the eastern SCB, it is developed for the 530–480 Ma Ross–Delamerian orogeny of the Terra Australis orogen along the Pacific margin of Gondwana (e.g., Cawood, 2005; Cawood and Buchan, 2007) and the Bhimphedian orogeny (550–470 Ma) of the North Indian Orogen along the Tethyan margin of Gondwana (e.g., Cawood et al., 2007). Wang et al. (2010) and Yu et al. (2007b) considered that the eastern SCB might be located at the northern margin of Gondwana linking Terra Australis orogen and Bhimphedian orogen during late early Paleozoic time. This link is also supported by (1) the similarity of detrital provenance and sedimentary sequences among the Northern India, Greater Himalaya, Lesser Himalaya and Cathaysia Blocks during late Neoproterozoic and early Paleozoic time (DeCelles et al., 2000; Gehrels et al., 2003; Myrow et al., 2006, 2009, 2010; Metcalfe, 2011; Yu et al., 2007a, 2007b; Wang et al., 2010), and (2) the unconformity between the Ordovician and Cambrian successions in northern India (e.g., Hughes, 2002; Myrow et al., 2009, 2010), Hainan and Yunkai Domains of the eastern Cathaysia (e.g., Guangdong BGMR, 1988; Wang et al., 2010; Zhang AM et al., 2011). Thus we propose that the Kwangsian intracontinental orogeny of the Yangtze and Cathaysia Blocks might have geodynamically resulted from the far-field response for the amalgamation of the Australian-Indian plate and the Cathaysia (also Indochina) Block along the northern margin of east Gondwana.

7. Conclusions

A comprehensively geochemical, zircon U–Pb geochronological and Hf isotopic study on the gneissoid granites along the Wugong, Wuyi and Yunkai Domains allows us to attach the following conclusions:

1) The gneissoid granites from the Wugong, Wuyi and Yunkai Domains gave zircon U–Pb ages of 415–457 Ma with a peak age of 436 Ma, indicating that these gneissoid rocks are of the Kwangsian origin rather than Precambrian basement traditionally thought.
2) These gneissoid samples are peraluminous with A/CNK of 1.02–1.36 and show a significant enrichment in LILE and LREE and a depletion in HFSE and HREE. They have high initial $^{87}Sr/^{86}Sr$ ratios and negative εNd(t) values. The zircons crystallized in the Kwangsian gneissoid granites gave εHf(t) values ranging from +2.4 to −19.4 (clustering at −1 to −12) and Hf model age of 1.1 to 2.1 Ga.
3) The Kwangsian gneissoid granites might have been derived from the product of bulk mixing of Proterozoic (probably with minor lower Paleozoic) crust materials with poor input of the juvenile mantle-derived magmas.
4) A good correlation is shown for the temporal and spatial patterns and protolith materials between the Kwangsian gneissoid granite and metamorphic rocks in the eastern SCB. These gneissoid granites might develop into an intracontinental tectonic regime related to the doubly crustal thickening and were mechanically linked to the middle Paleozoic far-field response to the assembly of the Australian–Indian plate with the Cathaysia Block.

Supplementary materials related to this article can be found online at doi:10.1016/j.lithos.2011.07.027.

Acknowledgments

We would like to thank X–P Xia for his help during the zircon U–Pb analyses. We are grateful to Profs. Stefan Jung, J. Charvet, Nelson Eby and an anonymous reviewer for their critical and constructive review, which led to major improvement of the manuscript. This study was jointly funded by the National Basic Research Program of China (2007CB411403), China Natural Science Foundation (40825009, 40830319 and 40772129), Hong Kong RGC Projects (7055/03P) and the Chinese Academy of Sciences (KZCX1-YW-15-1). We are grateful for the support from the Sin-British Fellowship Trust Visitorship

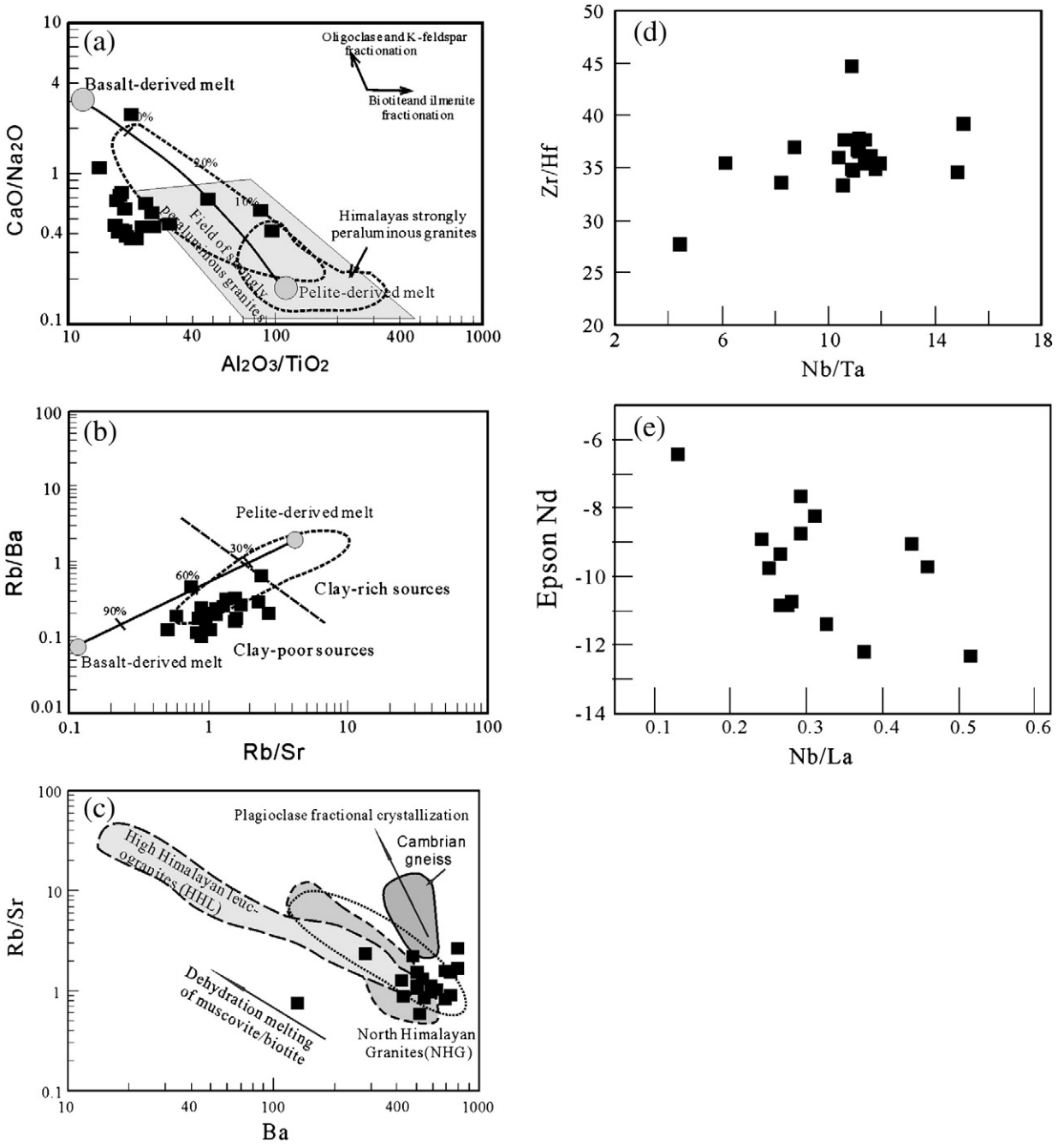

Fig. 17. Al_2O_3/TiO_2 versus CaO/Na_2O (a), Rb/Sr versus Rb/Ba (b), Rb/Sr versus Ba (c), Nb/Ta versus Zr/Hf (d) and Nb/La versus εNd(t) (e) for the Kwangsian gneissoid granites in the eastern South China Block. Fields of strongly peraluminous granites for all orogens and Himalayas are from Sylvester (1998). The mixing curve between the basalt- and pelite-derived melts in (a–b) is from Patiño-Douce and Harris (1998) and Sylvester (1998). Cambrian gneiss and peraluminous granite from the North Himalayan Granites (NHG) and High Himalayan leucogranites (HHL) in (f) are from Inger and Harris (1993) and Zhang et al. (2004). Symbols are the same as those in Fig. 17a.

2009–2010 to Y-J Wang and Coucher Foundation for the joint Laboratory between HKU and Guangzhou Institute of Geochemistry, Chinese Academy of Sciences. This is GIGCAS Publication No.1382 and a contribution to Guangzhou Institute of Geochemistry, Chinese Academy of Sciences.

References

Altherr, R., Holl, A., Hegner, E., Langer, C., Kreuzer, H., 2000. High-potassium, calc-alkaline plutonism in the European Variscides: northern Vosges (France) and northern Schwarzwald (Germany). Lithos 50, 51–73.

Anthony, E.Y., 2005. Source regions of granites and their links to tectonic environment: examples from the western United States. Lithos 80, 61–74.

Beard, J.S., Lofgren, G.E., 1991. Dehydration melting and water-saturated melting of basaltic and andesitic greenstones and amphibolites at 1, 3, and 6.9 kbar. Journal of Petrology 32, 365–401.

Cawood, P.A., 2005. Terra Australis Orogen: Rodinia breakup and development of the Pacific and Iapetus margins of Gondwana during the Neoproterozoic and Paleozoic. Earth Science Review 69 (3–4), 249–279.

Cawood, P.A., Buchan, C., 2007. Linking accretionary orogenesis with supercontinent assembly. Earth Science Review 82 (3–4), 217–256.

Cawood, P.A., Johnson, M.R.W., Nemchin, A.A., 2007. Early Paleozoic orogenesis along the Indian margin of Gondwana: tectonic response to Gondwana assembly. Earth and Planetary Sciences Letter 255 (1–2), 70–84.

Chappell, B.W., White, A.J.R., 1992. I- and S-type granites in the Lachlan fold belt. Transactions Royal Society of Edinburgh: Earth Sciences 83, 1–26.

Charvet, J., Shu, L.S., Shi, Y.S., Guo, L.Z., Faure, M., 1996. The building of south China: collision of Yangtze and Cathaysia Blocks, problems and tentative answers. Journal of Southeast Asian Earth Sciences 13 (3–5), 223–235.

Charvet, J., Cluzel, D., Faure, M., Caridroit, M., Shu, L.S., Lu, H.F., 1999. Some tectonic aspects of the pre-Jurassic accretionary evolution of East Asia. In: Metcalfe, I., Ren, J. S., Charvet, J., Hada, S. (Eds.), Gondwana Dispersion and Asian Accretion, IGCP 321 Final Results Volume. Balkema, pp. 37–65.
Charvet, J., Shu, L.S., Faure, M., Choulet, F., Wang, B., Lu, H.F., Breton, N.L., 2010. Structural development of the Lower Paleozoic belt of South China: genesis of an intracontinental orogen. Journal of Asian Earth Sciences 39, 309–330.
Chen, A., 1999. Mirror thrusting in the south China Orogenic belt: tectonic evidence from western Fujian, southeastern China. Tectonophysics 305, 497–519.
Chen, J.F., Jahn, B.M., 1998. Crustal evolution of southeastern China: Nd and Sr isotopic evidence. Tectonophysics 284, 101–133.
Chen, X., Rong, J.Y., Mitchell, C.E., Happer, D.A.T., Fan, J.X., Zhan, R.B., Zhang, Y.D., Li, R.Y., Wang, Y., 2000. Late Ordovician to earliest Silurian graptolite and brachiopod zonation from Yangtze Region, South China with a global correlation. Geological Magazine 137 (6), 623–650.
Chen, H.D., Hou, M.C., Xu, X.S., Tian, J.C., 2006. Tectonic evolution and sequence stratigraphic framework in South China during Caledonian. Journal of Chengdu University of Technology 33 (1), 1–8.
Chen, C.H., Lee, C.Y., Hsieh, P.S., Zeng, W., Zhou, H.W., 2008. Approaching the age problem for some metamorphosed Precambrian basement rocks and Phanerozoic granitic bodies in the Wuyishan area: the application of EMP monazite age dating. Geological Journal of China Universities 14 (1), 1–15.
Chen, X., Zhang, Y.D., Fan, J.X., Cheng, J.F., Li, Q.J., 2010. Ordovician graptolite-bearing strata in southern Jiangxi with a special reference to the Kwangsian Orogeny. Science in China (Earth Sciences) 53 (1), 1602–1610.
Culshaw, N., Gerbi, C., Marsh, J., 2010. Softening the lower crust: modes of syntransport transposition around and adjacent to a deep crustal granulite nappe, Parry Sound domain, Grenville Province, Ontario, Canada. Tectonics 29, TC5013. doi:10.1029/2009 TC002537.
DeCelles, P.G., Gehrels, G.E., Quade, J., LaReau, B., Spurlin, M., 2000. Tectonic implications of U–Pb zircon ages of the Himalayan orogenic belt in Nepal. Science 288, 497–499.
Ding, X., Zhou, X.M., Sun, T., 2005. The episodic growth of the continental crustal basement in South China: single zircon LA-ICPMS U–Pb dating of Guzhai granodiorite in Guangdong. Geological Review 51 (4), 383–392.
Dobosi, G., Kempton, P.D., Downes, H., Embey-Isztin, A., Thirlwall, M., Greenwood, P., 2003. Lower crustal granulite xenoliths from the Pannonian Basin, Hungary, Part 2: Sr–Nd–Hf–O isotope evidence for formation of continental lower crust by tectonic emplacement of oceanic crust. Contributions to Mineralogy and Petrology 144, 671–683.
Faure, M., Sun, Y., Shu, L., Monié, P., Charvet, J., 1996. Extensional tectonics within a subduction-type orogen: the case study of the Wugongshan dome (Jiangxi Province, southeastern China). Tectonophysics 263, 77–106.
Faure, M., Shu, L.S., Wang, B., Charvet, J., Choulet, F., Monié, P., 2009. Intracontinental subduction: a possible mechanism for the Early Paleozoic Orogen of SE China. Terra Nova. doi:10.1111/j.1365-3121.2009.00888.
Fujian BGMR (Bureau of Geology and Mineral Resources of Fujian Province), 1985. Regional Geology of the Fujian Province. Geological Publishing House, Beijing, pp. 1–610 (in Chinese with English abstract).
Gao, S., Lin, W.L., Qiu, Y.M., 1999. Contrasting geochemical and Sm–Nd isotopic compositions of Archaean metasediments from the Kongling high-grade terrain of the Yangtze craton: evidence for cratonic evolution and redistribution of REE during crustal anatexis. Geochimica et Cosmochimica Acta 13 (14), 2071–2088.
Gaudemer, Y., Jaupart, C., Tapponnier, P., 1988. Thermal control on postorogenic extension in collision belts. Earth and Planetary Science Letters 89 (1), 48–62.
Gehrels, G.E., Yin, A., Wang, X., 2003. Detrital zircon geochronology of the northeastern Tibetan plateau. Geological Society of America Bulletin 115, 881–896.
Gerbi, C., Culshaw, N.G., Marsh, J.H., 2010. Magnitude of weakening during crustal-scale shear zone development. Journal of Structural Geology 32, 107–117.
Griffin, W.L., Wang, X., Jackson, S.E., 2002. Zircon chemistry and magma genesis, SE China: in-situ analysis of Hf isotopes, Tonglu and Pingtan igneous complexes. Lithos 61, 237–269.
Guangdong, BGMR (Bureau of Geology and Mineral Resources of Guangdong Province), 1988. Regional Geology of the Guangdong Province. Geological Publishing House, Beijing, pp. 1–941 (in Chinese with English abstract).
Guangxi BGMR (Bureau of Geology and Mineral Resources of Guangxi Zhuang Autonomous Region), 1985. Regional Geology of the Guangxi Zhuang Autonomous Region. Geological Publishing House, Beijing, pp. 1–853 (in Chinese with English abstract).
Guo, L.Z., Shi, Y.S., Lu, H.F., Ma, S.R., Dong, H.G., Yang, S.F., 1989. The pre-Devonian tectonic patterns and evolution of South China. Journal of SE Asian Earth Sciences 3, 87–93.
Harrison, T.M., Grove, M., Lovera, O.M., Catlos, E.J., D'Andrea, J., 1999. The origin of Himalayan anatexis and inverted metamorphism: models and constraints. Journal of Asian Earth Sciences 17, 755–772.
Haynes, S.J., 1988. Structural reconnaissance of the Jiangnan geoanticline: a suspect terrane of compressional tectonic characteristics. In: Howell, D.G., Wiley, T.J. (Eds.), Proc. 4th Inter'l Tectonostratigraphic Terrane Conf. U.S. Geology Survey, Menlo Park, California, pp. 31–33.
Healy, B., Collins, W.J., Richards, S.W., 2004. A hybrid origin for Lachlan S-type granites: the Murrumbridgee batholith example. Lithos 79, 197–216.
Hsű, K.J., Li, J.L., Chen, H.H., Wang, Q.C., Sun, S., Sengör, A.M.X., 1990. Tectonics of South China: key to tectonics of South China: key to understanding west Pacific geology. Tectonophysics 193, 9–39.
Huang, J.Q., 1978. An outline of the tectonic characteristics of China. Eclogate Geologicate Helvetiae 71 (3), 611–635.
Huang, X., Depaolo, D.J., 1989. Study of sources of Paleozoic granittoids and the basement of South China by means of Sr–Nd isotope. Acta Petrologica Sinica 1, 28–36.
Huang, J.Q., Ren, J.S., Jiang, C.F., Zhang, Z.K., Qin, D.Y., 1987. Geotectonic evolution of China. Springer-Verlag, Berlin, pp. 1–203.
Huerta, A.D., Royden, L.H., Hodges, K.V., 1999. The effects of accretion, erosion and radiogenic heat on the metamorphic evolution of collisional orogens. Journal of Metamorphic Geology 17, 349–366.
Hughes, N.C., 2002. Late Middle Cambrian trace fossils from the Lejopyge armata horizon, Zanskar Valley, India, and the use of Precambrian/Cambrian ichnostratigraphy in the Indian subcontinent (Special Papers in) Palaeontology 67, 135–151.
Hunan, BGMR (Bureau of Geology and Mineral Resources of Hunan Province), 1988. Regional Geology of the Hunan Province. Geological Publishing House, Beijing, pp. 286–507 (in Chinese with English abstract).
Inger, S., Harris, N.B.W., 1993. Geochemical constraints on leucogranite magmatism in the Langtang Valley, Nepal Himalaya. Journal of Petrology 34, 345–368.
Jiangxi, BGMR (Bureau of Geology and Mineral Resources of Jiangxi Province), 1984. Regional Geology of the Jiangxi Province. Geological Publishing House, Beijing, pp. 1–921 (in Chinese with English abstract).
Jung, S., Hoernes, S., Mezger, K., 2000. Geochronology and petrogenesis of Pan-African, syntectonic, S-type and post- tectonic A-type granite(Namibia): products of melting of crustal sources, fractional crystallization and wall rock entrainment. Lithos 50, 259–287.
Labrousse, L., Hetényi, G., Raimbourg, H., Jlivet, L., Andersen, T.B., 2010. Initiation of crustal-scale thrusts triggered by metamorphic reactions at depth: insights from a comparison between the Himalayas and Scandinavian Caledonides. Tectonics 29, TC5002. doi:10.1029/2009TC002602.
Lambert, I.B., Wyllie, P.J., 1972. Melting of gabbro (quartz eclogite) with excess water to 35 kb, with geological applications. Journal of Geology 80 (6), 693–708.
Li, X.H., 1997. Timing of the Cathaysia Block formation: constraints from SHRIMP U–Pb zircon geochronology. Episodes 20 (3), 188–192.
Li, Z.X., 1998. Tectonic history of the major East Asian lithospheric blocks since the mid-Proterozoic: a synthesis. AGU Geodynamics Series, 27. American Geophysical Union, Washington, D.C., pp. 221–243.
Li, Z.X., Zhang, L., Powell, C.M., 1995. South China in Rodinia: part of the missing link between Australia–East Antarctica and Laurentia? Geology 23, 407–410.
Li, Z.X., Li, X.H., Zhou, H.W., Kinny, P.D., 2002. Grenvillian continental collision in south China: new SHRIMP U–Pb zircon results and implications for the configuration of Rodinia. Geology 2, 163–166.
Li, W.X., Li, X.H., Li, Z.X., 2005. Neoproterozoic bimodal magmatism in the Cathaysia Block of South China and its tectonic significance. Precambrian Research 136 (1), 51–66.
Li, Z.X., Li, X.H., Li, W.X., Ding, S.J., 2008. Was Cathaysia part of Proterozoic Laurentia? — new data from Hainan Island, South China. Terra Nova 20, 154–164.
Li, C., Chen, S.Y., Zhang, P.F., Zhang, Y., Wang, L., Bi, M.W., 2010a. Research of South China Caledonian intracontinental tectonic attribute. Journal of China University of Petroleum 34 (5), 18–24.
Li, L.M., Sun, M., Wang, Y.J., Xing, G.F., Zhao, G.C., Lin, S.F., Xia, X.P., Chan, L.S., Zhang, F.F., Wong, J., 2010b. U–Pb and Hf isotopic study of zircons from migmatised amphibolites in the Cathaysia Block: implications for the early Paleozoic peak tectonothermal event in Southeastern China. Gondwana Research. doi:10.1016/j.gr.2010. 03.009.
Li, Z.X., Li, X.H., Wartho, J.A., Clark, C., Li, W.X., Zhang, C.L., Bao, C.M., 2010. Magmatic and metamorphic events during the Early Paleozoic Wuyi–Yunkai Orogeny, southeastern South China: New age constraints and P–T conditions. GSA Bulletin 122 (5–6), 772–793.
Liu, B.J., Xu, X.S., 1994. Atlas of Lithofacies and Palaeogeography of South China (Sinian to Triassic). Science Press, Beijing, pp. 1–188.
Liu, X.M., Gao, S., Diwu, C.R., Ling, W.L., 2008. Precambrian crustal growth of Yangtze craton as revealed by detrital zircon studies. American Journal of Science 308, 421–468.
Ludwig, K.R., 2001. Sqiud 1.02: A User Manual. Berkeley Geochronological Center Special Publication, pp. 1–219.
Ma, L., Chen, H.J., Gan, K.W., Xu, X.S., Wu, G.Y., Ye, Z., Liang, X., Wu, S.H., Qiu, Y.Y., Zhang, P.L., Ge, P.P., 2004. Geotectonics and petroleum geology of marine sedimentary rocks in southern China. Geological Publishing House, Beijing, pp. 1–867.
Metcalfe, I., 2011. Tectonic framework and Phanerozoic evolution of Sundaland. Gondwana Research. doi:10.1016/j.gr.2010.02.016.
Miller, C.F., 1995. Are strongly peraluminous magmas derived from pelitic sedimentary sources? Journal of Geology 93, 673–689.
Myrow, P.W., Snell, K.E., Hughes, N.C., Paulsen, T.S., Heim, N.A., Parcha, S.K., 2006. Cambrian depositional history of the Zanskar Valley region of the Indian Himalaya: tectonic implications. Journal of Sedimentary Research 76, 364–381. doi:10.2110/jsr.2006.020.
Myrow, P.M., Hughes, N.C., Searle, M.P., Fanning, C.M., Peng, S.C., Parcha, S.K., 2009. Stratigraphic correlation of Cambrian–Ordovician deposits along the Himalaya: implications for the age and nature of rocks in the Mt. Everest region. Geological Society of American Bulletin 120, 323–332.
Myrow, P.M., Hughes, N.C., Goodge, J.W., Fanning, C.M., Williams, I.S., Peng, S.C., Bhargava, O.N., Parcha, S.K., Pogue, K.R., 2010. Extraordinary transport and mixing of sediment across Himalayan central Gondwanaland during the Cambrian–Ordovician. Geological Society of American Bulletin. doi:10.1130/B30123.1.
Nebel-Jacobsen, Y., Scherer, E.E., Munker, K., Mezger, K., 2005. Separation of U, Pb, Lu and Hf from single zircons for combined U–Pb dating and Hf isotope measurements by TIMS and MC-ICPMS. Chemical Geology 220, 105–120.
Patiňo-Douce, A.E., Harris, N., 1998. Experimental constraints on Himalayan anatexis. Journal of Petrology 39 (4), 689–710.

Patiño-Douce, A.E., Humphreys, E.D., Johnston, A.D., 1990. Anatexis and metamorphism in tectonically thickened continental crust exemplified by the Sevier hinterland, western North America. Earth and Planetary Science Letters 97, 290–315.
Qin, X.F., Pan, Y.M., Li, L., Li, R.S., Zhou, F.S., Hu, G.A., Zhong, F.Y., 2006. Zircon SHRIMP U–Pb geochronology of the Yunkai metamorphic complex in southeastern Guangxi, China. Geological Bulletin of China 25 (5), 553–559.
Qiu, Y.M., Gao, S., McNaughton, N.J., Groves, D.I., Ling, W.L., 2000. First evidence of >3.2 Ga continental crust in the Yangtze craton of South China and its implications for Archean crustal evolution and Phanerozoic tectonics. Geology 28 (1), 11–14.
Rapp, R.P., Watson, E.B., 1995. Dehydration melting of metabasalt at 8–32 kbar: implications for continental growth and crust-mantle recycling. Journal of Petrology 36, 891–931.
Ren, J.S., 1991. On the geotectonics of southern China. Acta Geologica Sinica (English Edition) 4 (2), 111–136.
Rong, J.Y., Chen, X., Harper, D.A.T., 2002. The latest Ordovician Hirnantia Fauna (Brachiopoda) in time and space. Lethaia 35, 231–249.
Rong, J.Y., Fan, J.X., Miller, A.I., Li, G.X., 2007. Dynamic patterns of latest Proterozoic- Paleozoic-early Mesozoic marine biodiversity in South China. Geological Journal 42, 431–454.
Rosenberg, C.L., Handy, M.R., 2005. Experimental deformation of partially melted granite revisited: implications for the continental crust. Journal of Metamorphic Geology 23, 19–28.
Rushmer, T., 1991. Partial melting of two amphibolites: contrasting experimental results under fluid-absent conditions. Contributions to Mineralogy and Petrology 107, 41–59.
Rutter, E.H., Mecklenburgh, J., 2006. The extraction of melt from crustal protoliths and the flow behavior of partially molten crustal rocks: an experimental perspective. In: Brown, M., Rushwer, T. (Eds.), Evolution and Differentiation of the Continental Crust. Cambridge University Press, pp. 385–430.
Schilling, F.R., Partzsch, G.M., Brasse, H., Schwarz, G., 1997. Partial melting below the magmatic arc in the central Andes deduced from geoelectromagnetic field experiments and laboratory data. Physics of the Earth and Planetary Interiors 103, 17–31.
Shen, W.Z., Ling, H.F., Li, W.X., Wang, D.Z., 1998. Sr and Nd isotope of Mesozoic granitoids in Jiangxi Province. Chinese Science Bulletin 43, 2653–2657.
Shu, L.S., Charvet, J., Shi, Y.S., Faure, M., Cluzel, D., Guo, L.Z., 1991. Structural analysis of the Nanchang–Wanzai sinistral ductile shear zone (Jiangnan region, South China). Journal of SE Asian Earth Sciences 6 (1), 13–23.
Shu, L.S., Faure, M., Wang, B., Zhou, X.M., Song, B., 2008a. Late Paleozoic–Early Mesozoic geological features of South China: response to the Indosinian collision events in Southeast Asia. Comptes Rendus Geoscience 340 (2–3), 151–165.
Shu, L.S., Yu, J.H., Jia, D., Wang, B., Shen, W., Zhang, Y.Q., 2008b. Early Palaeozoic orogenic belt in the eastern segment of South China. Geological Bulletin of China 27, 1581–1593.
Shui, T., 1987. Tectonic framework of the southeastern China continental basement. Scientia Sinica B30, 414–421 (In Chinese with English Abstract).
Streule, M.J., Searle, M.P., Waters, D.J., Horstwood, M.S.A., 2010. Metamorphism, melting, and channel flow in the Greater Himalayan Sequence and Makalu leucogranite: constraints from thermobarometry, metamorphic modeling, and U–Pb geochronology. Tectonics 29, TC5011. doi:10.1029/2009TC002533, 2010.
Sun, T., 2006. Distribution of granites from South China and its petrogenesis. Geochimica et Cosmochimica Acta 70 (18 Suppl. 1), A626.
Sun, S.S., McDonough, W.F., 1989. Chemical and isotopic systematics of oceanic basalts: implication for mantle composition and process. In: Sauders, A.D., Norry, M.J. (Eds.), Magmatism in the ocean Basins: Geol. Soc. Spec. Pub., 42, pp. 313–345.
Sylvester, P.J., 1998. Postcollisional strongly peraluminous granites. Lithos 45, 29–44.
Taylor, S.R., McLennan, S.M., 1985. The continental crust: its composition and evolution. Oxford Press (Blackwell), pp. 1–312.
Ting, W.K., 1929. The orogenic movement in China. Bullet. Geological Society of China 8 (1), 151–170.
Tompson, A.B., 1996. Fertility of crustal rocks during anatexis. Transactions of the Royal Society of Edinburgh: Earth Sciences 87, 1–10.
Vanderhaeghe, O., Teyssier, C., 2001. Partial melting and flow of orogens. Tectonophysics 342, 451–472.
Vielzeuf, D., Schmidt, N.W., 2001. Melting relations in hydrous systems revisited: application to metapelites, metagreywackes and metabasalts. Contributions to Mineralogy and Petrology 141, 251–267.
Wan, Y.S., Liu, D.Y., Xu, M., Zhuang, J., Song, B., Shi, Y., Du, Y.L., 2007. SHRIMP U–Pb zircon geochronology and geochemistry of metavolcanic and metasedimentary rocks in Northwestern Fujian, Cathaysia Block, China: tectonic implications and the need to redefine lithostratigraphic units. Gondwana Research 12 (1–2), 166–183.
Wan, Y.S., Liu, D.Y., Wilde, S.M., Cao, J.J., Chen, B., Dong, C.Y., Song, B., Du, L.L., 2010. Evolution of the Yunkai terrane, South China: evidence from SHRIMP zircon U–Pb dating, geochemistry and Nd isotope. Journal of Asian Earth Science 37, 140–153.
Wang, J., Li, Z.X., 2003. History of Neoproterozoic rift basins in South China: implications for Rodinia breakup. Precambrian Research 122 (1–4), 141–158.
Wang, Y.J., Fan, W.M., Guo, F., Peng, T.P., Li, C.W., 2003. Geochemistry of Mesozoic mafic rocks around the Chenzhou–Linwu fault in South China: implication for the lithospheric boundary between the Yangtze and the Cathaysia Blocks. International Geology Review 45 (3), 263–286.
Wang, Y.J., Fan, W.M., Sun, M., Liang, X.Q., Zhang, Y.H., Peng, T.P., 2007a. Geochronological, geochemical and geothermal constraints on petrogenesis of the Indosinian peraluminous granites in the South China Block: a case study in the Hunan Province. Lithos 96, 475–502.
Wang, Y.J., Fan, W.M., Zhao, G.C., Ji, S.C., Peng, T.P., 2007b. Zircon U–Pb geochronology of gneissic rocks in the Yunkai massif and its implications on the Caledonian event in the South China Block. Gondwana Research 12 (4), 404–416.
Wang, Y.J., Fan, W.M., Cawood, P.A., Li, S.Z., 2008. Sr–Nd–Pb isotopic constraints on multiple mantle domains for Mesozoic mafic rocks beneath the South China Block hinterland. Lithos 106, 297–308.
Wang, Y.J., Zhang, F.F., Fan, W.M., Zhang, G.W., Chen, S.Y., Cawood, P.A., Zhang, A.M., 2010. Tectonic setting of the South China Block in the early Paleozoic: resolving intracontinental and ocean closure models from detrital zircon U–Pb geochronology. Tectonics 29. doi:10.1029/2010TC002750.
Wolf, M.B., Wyllie, P.J., 1991. Dehydration-melting of solid amphibolite at 10 kbar: textural development, liquid interconnectivity and applications to the segregation of magmas. Mineralogy and Petrology 44, 151–179.
Wu, F.J., Zhang, F.R., 2003. Features and genesis of Caledonian granites in the Wugong in the eastern segment of the northern margin of South China. Geology of China 30 (2), 166–172 (In Chinese with English abstract).
Wu, F.Y., Yang, Y.H., Xie, L.W., Yang, J.H., Xu, P., 2006. Hf isotopic compositions of the standard zircons and baddeleyites used in U–Pb geochronology. Chemical Geology 234, 105–126.
Xia, X.P., Sun, M., Zhao, G.C., Li, H.M., Zhou, M.F., 2004. Spot zircon U–Pb isotope analysis by ICP-MS coupled with a frequency quintupled (213 nm) Nd-YAG laser system. Geochemical Journal 38, 191–200.
Xiang, H., Zhang, L., Zhou, H.W., Zhong, Z.Q., Zeng, W., Liu, R., Jin, S., 2008. U–Pb zircon geochronology and Hf isotope study of metamorphosed basic-ultrabasic rocks from metamorphic basement in southwestern Zhejiang: the response of the Cathaysia Block to Indosinian orogenic event. Science in China (Series D-Earth Science) 51 (6), 788–800.
Xu, X.S., Xu, Q., Pan, G.T., 1996. The continental evolution of southern China and its global comparison. Geol. Pub. House, Beijing, pp. 10–12.
Xu, X.S., O'Reilly, S.Y., Griffin, W.L., Deng, P., Pearson, N.J., 2005. Relict Proterozoic basement in the Nanling Mountains (SE China) and its tectonothermal overprinting. Tectonics 24 (2), TC2003.
Yang, D.S., Li, X.H., Li, W.X., Liang, X.Q., Long, W.G., Xiong, X.L., 2010. U–Pb and ^{40}Ar–^{39}Ar geochronology of the Baiyunshan gneiss (central Guangdong, south China): constraints on the timing of early Paleozoic and Mesozoic tectonothermal events in the Wuyun (Wuyi–Yunkai) Orogen. Geological Magazine 147, 481–496.
Yu, J.H., Zhou, X.M., Zhao, L., et al., 2003. Discovery and implications of granulite facies metamorphic rocks in the eastern Nanling, China. Acta Petrologica Sinica 19 (3), 461–467 (In Chinese with English abstract).
Yu, J.H., Zhou, X.M., O'Reilly, S.Y., 2005. Formation history and protolith characteristics of granulite facies metamorphic rock in Central Cathaysia deduced from U–Pb and Lu–Hf isotopic studies of single zircon grains. Chinese Science Bulletin 50 (18), 2080–2089.
Yu, J.H., O'Reilly, S.Y., Wang, L.J., Griffin, W.L., Jiang, S.Y., Wang, R.C., Xu, X.S., 2007a. Finding of ancient materials in Cathaysia and implication for the formation of Precambrian crust. Chinese Science Bulletin 52 (1), 13–22.
Yu, J.H., Wang, L.J., Wei, Z.Y., Sun, T., Shu, L.S., 2007b. Phanerozoic metamorphic episodes and characteristics of Cathaysia Block. Geological Journal of China Universities 1 (5), 474–483.
Yu, J.H., Wang, L.J., Griffin, W.L., O'Reilly, S.Y., Zhang, M., Li, C.Z., Shu, L.S., 2009. A Paleoproterozoic orogeny recorded in a long-lived cratonic remnant (Wuyishan terrane), eastern Cathaysia Block, China. Precambrian Research 174 (3–4), 347–363.
Yu, J.H., O'Reilly, S.Y., Wang, L.J., Griffin, W.L., Zhou, M.F., Zhang, M., Shu, L.S., 2010. Components and Episodic growth of Precambrian crust in the Cathaysia Block, South China: evidence from U–Pb ages and Hf isotopes of zircons in Neoproterozoic sediments. Precambrian Research 181 (1–4), 97–114.
Zen, E., 1986. Aluminum enrichment in silicate melts by fractional crystallization: some mineralogic and petrographic constrains. Journal of Petrology 27, 1095–1117.
Zeng, Y., Liu, Q.A., 2000. Caledonian granites in the western Wuyi and inversion of the Orogenic process. Regional Geology of China 19 (4), 344–349 (In Chinese with English abstract).
Zeng, W., Zhang, L., Zhou, H.W., Zhong, Z.Q., Xiang, H., Liu, R., Jin, S., Lu, X.Q., Li, C.Z., 2008. Caledonian reworking of Paleoproterozoic basement in the Cathaysia Block: constraints from zircon U–Pb dating, Hf isotopes and trace elements. Chinese Science Bulletin 53 (6), 895–904.
Zhang, Z.J., Wang, Y.H., 2007. Crustal structure and contact relationship revealed from deep seismic sounding data in South China. Physics of the Earth and Planetary Interiors 165, 114–126.
Zhang, H.F., Harris, N., Parrish, R., Kelley, S., Zhang, L., Rogers, N., Argles, T., King, J., 2004. Causes and consequences of protracted melting of the mid-crust exposed in the North Himalayan antiform. Earth Planetary of Science Letter 228, 195–212.
Zhang, A.M., Wang, Y.J., Fan, W.M., Zhang, F.F., Zhang, Y.Z., 2010a. LA-ICPMS zircon U–Pb geochronology and Hf isotopic compositions of Caledonian granites from the Qingliu area, Southwest Fujian. Geotectonica et Metallogenia 34 (3), 408–418.
Zhang, F.F., Wang, Y.J., Fan, W.M., Zhang, A.M., Zhang, Y.Z., 2010b. LA-ICPMS zircon U–Pb geochronology of late Early Paleozoic granites in eastern Hunan and western Jiangxi provinces, South China. Geochimica 39 (5), 414–426.
Zhang, A.M., Wang, Y.J., Fan, W.M., Zhang, F.F., Zhang, Y.Z., 2011. LA-ICPMS zircons U–Pb geochronology and Hf isotopic composition of the Taoxi migmatite (Wuping): constrains on the formation age of the Taoxi complex and the Yu'nan event. Geotectonica et Metallogenia 35 (1), 64–72.
Zhao, G.C., Cawood, P.A., 1999. Tectonothermal evolution of the Mayuan assemblage in the Cathaysia Block: new evidence for Neoproterozoic collisional-related assembly of the South China craton. American Journal of Science 299, 309–339.
Zhejiang, BGMR(Zhejiang Bureau of Geology and Mineral Resources), 1996. Stratigraphy of Zhejiang Province. China University Geosciences Press, Beijing, China. (In Chinese with English abstract).
Zhou, X.M., 2003. My thinking about granite geneses of South China. Geological Journal of China Universities 9 (4), 556–565 (In Chinese with English abstract).
Zhou, X.M., Sun, T., Shen, W.Z., Shu, L.S., Niu, Y.L., 2006. Petrogenesis of Mesozoic granitoids and volcanic rocks in South China: a response to tectonic evolution. Episodes 29 (1), 26–33.
Zhou, X.M., Chen, P.R., Xu, X.S., 2007. Petrogenisis of late Mesozoic granite and dynamic evolution of Lithosphere in Nanling Region. Science Press, Beijing, pp. 1–691 (In Chinese).